



# Post-Fire Analysis of Thermally Sprayed Coatings: Evaluating Microstructure, Mechanical Integrity, and Corrosion Behavior

Ratna Divya Yasoda<sup>a</sup>, Nour Hakim<sup>b</sup>, Ying Huang<sup>a\*</sup>, and Xiaoning Qi<sup>c</sup>

- 1 Department of Civil, Construction, and Environmental Engineering., North Dakota State University, Fargo, USA; ratna.yasoda@ndus.edu
- Department of Mechanical Engineering, University of Nevada, Las Vegas, USA; Hakimn1@unlv.nevada.edu
- Department of Coatings and Polymeric Materials, North Dakota State University, Fargo, USA; xiaoning.qi@ndsu.edu
- Correspondence: ying.huang@ndsu.edu

Abstract: This paper examines the impact of fire on the microstructural, mechanical, and corrosion behavior of wire-arc sprayed zinc, aluminum, and Zn-Al pseudo alloy coatings. The steel plates coated with these materials were subjected to temperatures in increments of 100°C, starting from 300°C and continuing until they failed. Microstructural characterization, microhardness, abrasion resistance, and electrochemical impedance studies were performed on the post-fire coatings. The findings from this study show that heat has a positive impact on the performance of zinc and Zn-Al pseudo alloy coatings when they were exposed to temperatures up to 400°C, while aluminum coatings maintain their performance up to 600°C. However, above these temperatures, the effectiveness of coatings was observed to decline, primarily due to increased high-temperature oxidation, porosity, and decreased microhardness, abrasion resistance, and corrosion protection performance. Based on the findings from this study, appropriately sealed thermal spray-coated steel components can be reused after exposure to fire up to a specific temperature depending on the coating material.

Keywords: Fire; Residual life of coatings; Wire-arc spray process; Microstructure; Zinc; Aluminum; and High-temperature oxidation.

Introduction

staff during production. Academic Editor: Firstname Last-

Citation: To be added by editorial

Received: date Revised: date Accepted: date Published: date



Copyright: © 2022 by the authors. Submitted for possible open access publication under the terms and conditions of the Creative Commons (CC BY) (https://creativecommons.org/license s/by/4.0/).

The need for engineering steel in the construction of infrastructure has grown and necessitated the application of diverse steel classifications, such as those with lower carbon content, those of higher strength, and ultra-high strength To prevent corrosion damage and extend the lifespan of these steel structures especially, in offshore, marine, and industrial settings, metallic protective coatings are applied [1]. Due to their desirable protection performance, metallic coatings of zinc, aluminum, and their respective alloys are commonly applied for protecting steel structures against corrosion. Among the various zinc-aluminum alloys, Zn-15Al (85 wt.% zinc and 15 wt.% aluminum) is a commonly used one which is known to offer excellent corrosion protection through both barrier action and cathodic protection functionalities. For the application of these coatings, thermal spray technology, specifically, wire-arc is gaining popularity among a range of coating application methods due to its flexibility to achieve desired coating thickness, and most importantly high processing speeds [2]. Several studies have explored the mechanical properties and corrosion performance of these thermally sprayed zinc and aluminum coatings, demonstrating the effective corrosion protection mechanisms offered by these coatings in chloride environments. In addition to the Zn-15Al coatings, wire-arc sprayed Zn-Al pseudo alloy coatings are also gaining popularity which enables the flexibility to change the composition of zinc and aluminum in the

Processes 2023, 11, x. https://doi.org/10.3390/xxxxx

www.mdpi.com/journal/processes

4 5

> 12 14 15

11

16 17 18

19 20 21

22 23

24

25

26

27

41 43

47

48

49

50

51

53

55

56

57

58

59

60

61

62

63

65

67

68

69

70

71

72

73

74

75

76

77

78

79

80

81

83

84

85

86

87

88

89

90

91

92

93

94

95

96

coating microstructure without the need for pre-alloying of the wires. According to recent studies, these pseudo-alloy coatings of zinc and aluminum with an aluminum content of 30 to 40 wt.% are excellent candidates for corrosion mitigation in steel structures [3-5].

For steel structures, in addition to corrosion, fire is another critical hazard, particularly in structures such as offshore platforms, oil, and gas pipelines, and bridges that are more susceptible to fire [6,7]. Over the last decade, the oil and gas pipeline industry has experienced around 1,200 fire accidents resulting in an economic loss of \$5.4 billion and fatalities [8]. In addition, incidents such as tanker truck accidents, and wild and bushfires [9,10] can also cause fire-induced damage to transportation assets like bridges [11]. It has been observed that the mechanical properties of steel sections become compromised following exposure to fire, with the degree of ineffectiveness dependent on the temperature of the fire. [12]. However, several published works investigating the behavior of steels following fire exposure have shown that yield strength, modulus of elasticity, and ultimate tensile strength of different grades of steels remain unaffected when subjected to temperatures up to  $600^{\circ}$ C [13,14].

These post-fire studies on steel were conducted on bare/uncoated steel members, however, the structural steel members are usually safeguarded by protective coatings to prevent corrosion. These anticorrosive coatings can be either metallic or polymer-based or a combination of both materials. [15,16]. Thus, it is imperative to examine the postfire properties of the coated steels when exposed to fire. While there have been advancements in creating high-temperature resistant polymer coatings, conventional polymer-based anti-corrosive coatings like epoxies and polyurethanes typically degrade above 200°C and may not survive high-fire temperatures. On the other hand, anticorrosive metallic coatings of zinc, and aluminum have much higher melting points (420°C for zinc and 660°C for aluminum) and should survive elevated temperatures of fire. However, there are only a few studies available on how these metallic coatings behave when exposed to high fire temperatures. For instance, a study by Graig et al. [17] demonstrated that hot-dip galvanization can offer passive protection to structural steels during fire exposure. The study also showed that heat development was slower for galvanized steel compared to uncoated steel. Similarly, the performance of hot-dip galvanized steel members was examined by McLean et al. [18] during bushfires. The results of the work suggested that for a recorded temperature of 675°C, the galvanized coating remained intact.

These aforementioned studies were solely focused on galvanized steel and information on post-fire microstructural changes, mechanical integrity, and electrochemical corrosion behavior of the coated steel was not available, especially, for the thermally sprayed corrosion protective coatings of zinc and aluminum. As mentioned previously, since thermally sprayed Zn-15Al coatings are commonly applied for corrosion protection, the authors examined this coating's post-fire behavior [19]. The results of the study indicated that the protective properties of the wire-arc sprayed Zn-15Al coatings were remain unaffected until 600°C exposure suggesting their probable reuse. When subjected to temperatures beyond 600°C, the coating lost its integrity and failed by cracking. In light of the promising outcomes of the post-fire performance evaluation of Zn-15Al coatings, the present work aims to explore three other popular wire-arc sprayed coatings mentioned earlier, namely zinc, aluminum, and Zn-Al pseudo alloy coatings. Thus, this paper presents the efficacy of these wire-arc sprayed coatings on structural steel when subjected to simulated high-fire temperatures, by analyzing the changes through physical observations, microstructural characterization, and mechanical, and electrochemical tests. The following sections of the manuscript delve into the specifics of the experimental design and present significant observations and results.

100

101

102

103

105

107

108

109

110

111

112

114

115

116

118

119

120

121

122

123

124

125

126

127

128

130

132

134

135

136

# **Coatings Application Procedure**

In this study, the wire-arc spray gun (Thermion, USA) with robotic arm setup was used to apply three different coatings, namely pure zinc (Zn), pure aluminum (Al), and Zn-Al pseudo alloy coatings, onto ASTM A 36 steel plates of size 50 mm x 50 mm. Wirearc process employs two consumable feedstock wires (which make up the material to be coated) that are given opposite electric charges and are fed close together. This generates an electric arc causing the wires to melt. Using compressed air, molten material is sprayed onto the substrate steel to form a coating. This study utilized commercially available 1.6 mm diameter pure zinc, and pure aluminum wires, as two feedstock wires in the spray gun to produce Zn and Al coatings, respectively. On the other hand, for the production of Zn-Al pseudo alloy coating, one pure Zn wire, and one pure Al wire were used on opposite sides of the spray gun as feedstock wires. With this setup, both metal wires were melted simultaneously, resulting in the production of a Zn-Al pseudo-alloy coating [4]. The steel plates were grit blasted prior to the coating deposition using alumina to improve the adhesion. The parameters of the wire-arc spray process are detailed in Table 1. The resulting coatings, including Zn, Al, and Zn-Al pseudo alloy, had thicknesses of 220  $\pm$  50  $\mu$ m, 200  $\pm$  50  $\mu$ m, and 250  $\pm$  50  $\mu$ m, respectively.

**Table 1.** Wire-arc process parameters.

Parameter	Value, Unit		
Spray distance	180 mm		
Arc Voltage	32 V		
Current	225 Amps		
Spray air pressure	0.62 MPa		
Substrate temperature	82°C		
Number of passes	2		

#### **High-temperature Testing of the Coatings**

The coated steel specimens were heated using an electrically powered furnace (Thermal Systems Inc, CA, USA) to simulate fire temperatures. The temperature of the specimens was gradually increased from room temperature up to a chosen level, which varied between 300°C and the point where a noticeable failure was observed with increments of 100°C. The initial test temperature of 300°C was chosen considering the melting points of zinc and aluminum which are 420°C and 660°C respectively. Additionally, based on the Zn-Al binary phase diagram no major phase changes occur in Zn-Al alloys below 280°C [20]. Temperatures lower than 300°C were not investigated in this study, as the electric furnace utilized has a tolerance range of ± 20°C. The heating process was carried out in the furnace at a rate of 10 to 15°C/min, which has been employed in various previous investigations aimed at examining the post-fire behavior and properties of engineering metals [21]. To maintain consistency with earlier research conducted on uncoated structural steels, the same heating rate was used in this work. Once the target temperature was reached, the samples were left in the furnace at that temperature for an hour to allow proper heat distribution in the samples. After this duration, the samples were taken out of the furnace and allowed to cool to room temperature outside. Once the cooling process was complete, the coatings were analyzed for alterations in microstructure and porosity. Furthermore, the effect of temperature on mechanical characteristics such as microhardness and abrasion resistance was investigated to examine the changes in the coatings' mechanical stability. Finally, the changes in coatings' corrosion protection behavior were studied through electrochemical studies.

#### Morphology and Microstructural Characterization

Studies show that exposing engineering metals and metallic coating to elevated temperatures can alter their microstructural characteristics, including the composition of metallurgical phases, morphology, grain size, etc. These alterations in the microstructure can have a considerable impact on the efficiency of the coating compared to its original, non-exposed/as-deposited state [14]. To understand these changes, a variety of material characterization tests were conducted. The outcomes of various characterization tests are incredibly useful in evaluating the coating's integrity and comprehending the microstructural changes that impact the mechanical and electrochemical performance of the coatings.

Scanning electron microscope (SEM) imaging was performed on the surface and cross sections of Zn, Al, Zn-Al pseudo alloy coatings in the un-exposed state and after cooling from varying high temperatures to investigate potential changes in microstructural features, high-temperature oxidation, and porosity. The SEM imaging was carried out using a JOEL JSM-6490 LV operated at 15kV. In addition, energy dispersive x-ray spectroscopy (EDS) which is available in the SEM was utilized to analyze the changes in the coatings' chemical composition and to perform the elemental mapping. Porosity changes in the coatings were estimated using Image J software. To calculate the porosity of the coatings, a minimum of six micrographs of a particular specimen that had been subjected to a specific temperature were utilized. In addition, X-ray diffraction analysis (XRD) was utilized to investigate the metallurgical phases that exist on the surface of the coatings in both as-deposited conditions and after being cooled from exposure to different elevated temperatures. XRD analysis was conducted using a Bruker D8 Discover diffractometer. The resulting XRD peaks were identified as per the inorganic crystal structure database (ICSD).

# **Mechanical Properties Evaluation**

Microhardness and abrasion resistance tests were performed in this study to assess how an increase in the exposure temperature influences the crucial mechanical properties of the coatings, including their hardness and ability to resist abrasion. The Vickers test was employed to measure the microhardness of the coatings.

The test was conducted using an applied load of 100 gram-force and an indentation time of 15 sec. The Vickers hardness (HV) was determined by optically measuring the lengths of the imprints left by the indenter, and then converting these measurements to HV using the formula as follows:

$$HV = 1.854 \times (F/D^2)$$
 (Eq 1)

where F represents the applied load in kgf and  $D^2$  corresponds to the projected indentation area measured in square millimeters ( mm<sup>2</sup>).

The abrasion resistance indicates the coating's ability to withstand disintegration and cutting by hard abrasives. Despite being a widely used method for measuring wear, the pin-on-disk test was found to be challenging in the present study, as the test required an average surface roughness below 0.8  $\mu m$  [22] (which is required as per ASTM G99-17) on the entire coating surface (50 mm x 50 mm) of these thinner coatings (less than 250  $\mu m$  thick) without exposing the substrate steel was observed to be a difficult task. Therefore, sandpaper abrasion test was utilized to determine the abrasion resistance of the coatings in their un-exposed state and after cooling from high-temperature exposures. The abrasion resistance of the coating is assessed in the sandpaper abrasion test by subjecting it to an applied stress of a specific magnitude [23]. In this study, the test specimen was subjected to the normal stress of 3.3 kPa by applying a weight of 600 grams on top of it. The coating surface (50 mm x 50 mm) was placed on 220-grit sandpaper of size 29.7 cm x 21 cm. To conduct the

190

191

192

193

194

195

196

197

198

199

200

201

202

203

204

205

206

207

208

209

210

211

213

214

215

216

217

218

219

220

221

222

223

224

225

226

227

228

229

test each of the three coating specimens manually moved back and forth over the sandpaper which was considered one cycle of abrasion. The weights of the specimens were measured before and after 30 cycles of abrasion to determine the changes in the coating's wear/abrasion loss with an increase in the exposed temperature. The percentage abrasion loss in the coating was used to evaluate the abration resistance.

#### **Electrochemical Studies**

Thermally sprayed zinc and aluminum coatings are commonly used in harsh and corrosive environments because they provide excellent protection to the underlying steel substrate. Given that corrosion is an electrochemical phenomenon, it is crucial to assess the alterations in the coating's electrochemical properties following exposure to elevated temperatures. To achieve this objective, the electrochemical impedance spectroscopy (EIS) technique was utilized in this study [24, 25]. EIS measures the resistance of the coating to the flow of electrons known as impedance in the corrosion system across a range of frequencies. By creating an impedance spectrum of the system over various frequencies, the coating's corrosion behavior and kinetics can be examined [26]. The coated steel specimen being investigated was used as the working electrode (WE), a platinum mesh was utilized as the counter electrode (CE), and a saturated calomel electrode functioned as the reference electrode (RE). To eliminate external interferences, the electrochemical cell was placed in a Faraday cage throughout the testing process.

The tests were performed on a working electrode area of 1 cm² and 3.5 wt.% NaCl solution was used as an electrolyte. The measurements were taken by applying a 3-mV amplitude sinusoidal voltage signal at a range of frequencies from 100kHz to 0.01 Hz. A minimum of five samples corresponding to each temperature level were tested to ensure the repeatability of the results.

## **Results and Discussion**

After cooling each of the three sets of coatings from their respective elevated temperatures, digital images were captured for the Zn, Al, and Zn-Al pseudo alloy coatings which are presented in Figures 1 to 3, respectively. As seen in Figure 1, Zn coatings did not exhibit any visible signs of damage or discoloration until they were cooled from 400°C. However, when they cooled from 500°C, the coatings turned yellow as a result of the formation of oxidation products of zinc [27]. Furthermore, the coating also lost its integrity and crumbled upon touch, likely due to the low melting point of Zn (420°C) and causing excessive oxidation beyond this point. Therefore, temperatures higher than 500°C were not investigated for Zn coatings. On the other hand, Al coatings remained intact and didn't display any signs of disintegration or color change up to 600°C exposure which can be seen in Figure 2. The Al coatings showed some discoloration upon cooling from 700°C exposure, but they remained sturdy and did not crumble into powder when touched (see Figure 2 (f)). When cooled from 800°C exposure, the surface of the Al coatings appeared heavily discolored and turned extremely fragile, collapsing under the slightest touch. Thus, temperatures higher than 800°C were not taken into consideration for Al coatings.

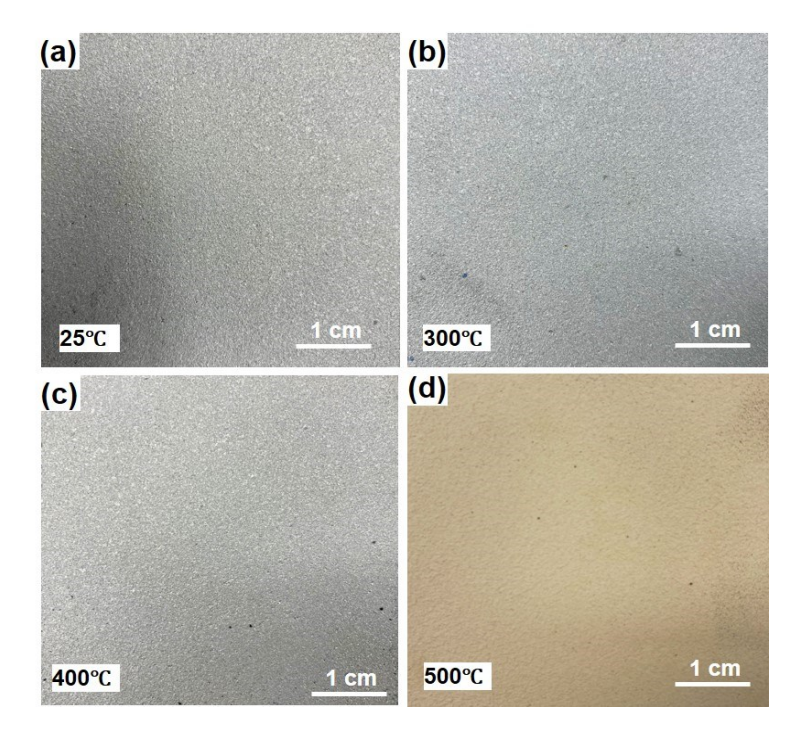


**Figure 1.** The digital images of Zn coating: a) at 25°C, and after exposure to b) 300°C, c) 400°C, and d) 500°C.

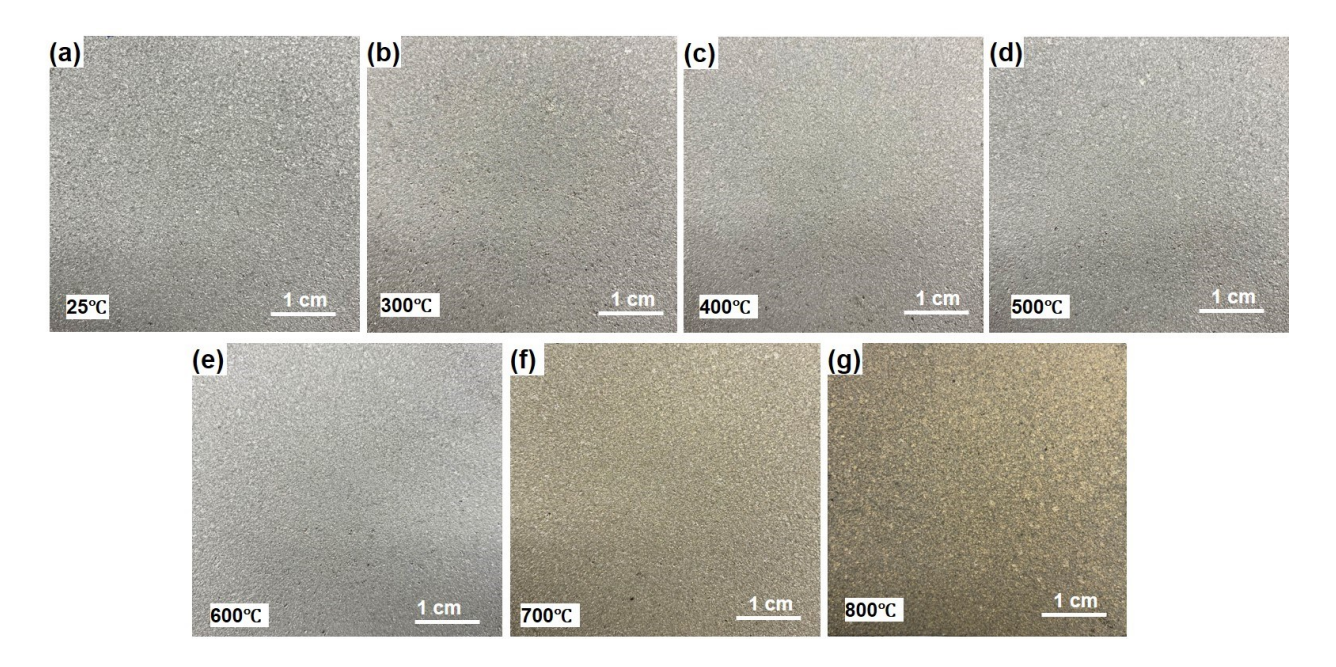


**Figure 2.** The digital images of Al coating: a) at 25°C and after exposure to b) 300°C, c) 400°C, d) 500°C, e) 600°C, f) 700°C, and g) 800°C exposures.

The Zn-Al pseudo alloy coatings showed minor discoloration and did not display any significant signs of delamination, heavy oxidation, or surface cracking until they were cooled from an exposed temperature of 500°C. However, when cooled from a 600°C exposure, the coatings failed in the form of surface cracking. The cracking mode of failure in Zn-Al pseudo alloy coatings can be attributed to various factors, such as the thermal incompatibility between Zn and Al, high-temperature oxidation, and other possible microstructural changes [20]. In summary, the visible mode of failure observed for

244

245

246

247

248

249

250

251

252

253

254

255

256

257

258

259

260

261

262

263

264

265

266

268

269

270

271

pure Zn, and pure Al coatings was the transformation of the coatings into a powdery substance/residue which can be attributed to high-temperature oxidation, while Zn-Al pseudo alloy coatings by cracking due to the difference in coefficient of thermal expansions of Zn and Al, in addition to the high-temperature oxidation. It can also be noted that the failure temperatures of the coatings are closely tied to the melting points of the corresponding metals.

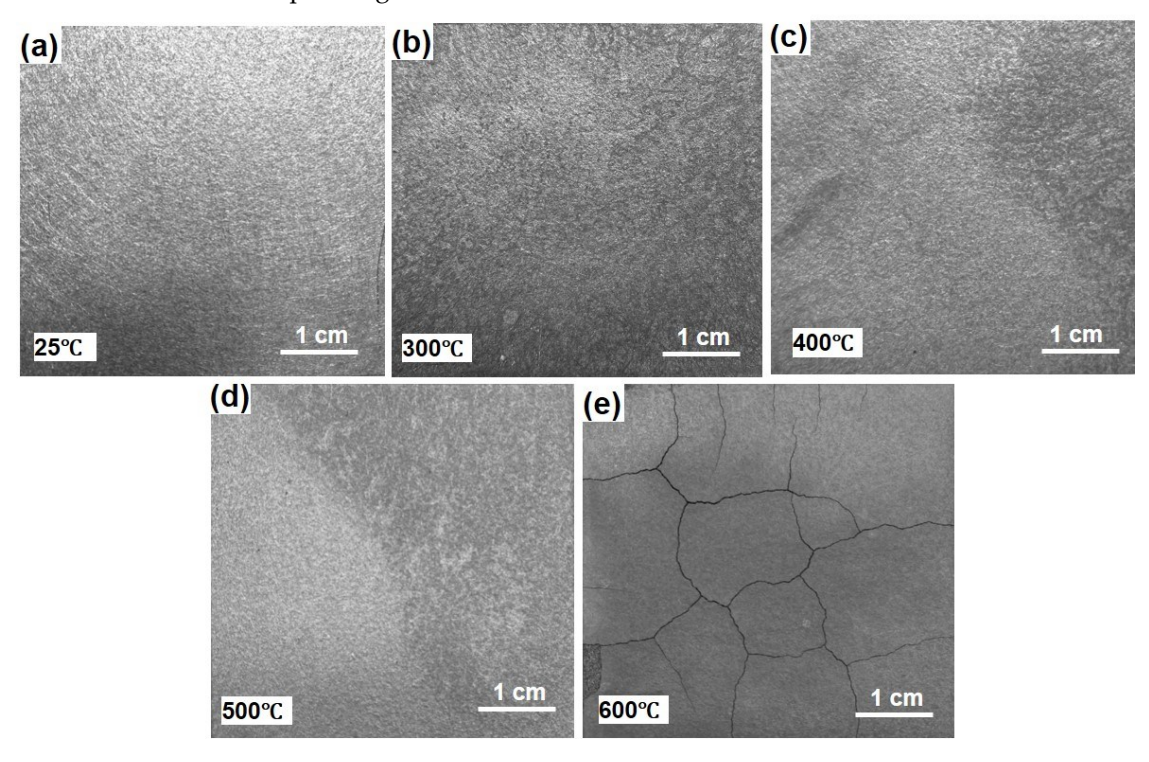


**Figure 3.** The digital images of Zn-Al pseudo alloy coating: a) at 25°C, and after exposure to b) 300°C, c) 400°C, d) 500°C, and e) 600°C.

# **SEM and EDS Analyses**

Figure 4 displays surface micrographs of Zn coatings at 1,000 X magnification in un-exposed conditions after they were cooled from 300°C and 400°C exposures. The micrographs in Figures 4 (a) to (c) show the pores and splat boundaries which are an inherent property of thermal spray coatings. It is worth noting that, as the exposure temperature increased, the number of pores and splat boundaries were reduced. The transformation in the microstructure of zinc caused by melting and restructuring can account for this, which potentially helped fill in the pores and reduce porosity [28]. Therefore, the micrographs taken on the surface of the Zn coatings did not reveal any signs of microstructural deterioration such as cracks, voids, and other irregularities that can impact the coating's desirable performance. The cross-section micrographs of the Zn coatings which were cooled from various elevated temperatures, along with that the corresponding EDS maps of oxygen are shown in Figure 5 to demonstrate the changes in the extent of oxidation in the coating microstructure with a rise in the temperature of exposure. As seen in Figures 5 (a) to (c), the cross-section didn't show any signs of delamination or excessive oxidation after exposure to 300°C and 400°C temperatures at the considered magnification. The SEM imaging and EDS analysis of the Zn coatings show no apparent signs of damage. However, it is crucial to consider these results in conjunction with other characterization results to conclude the reusability of Zn coatings after exposure to fire.

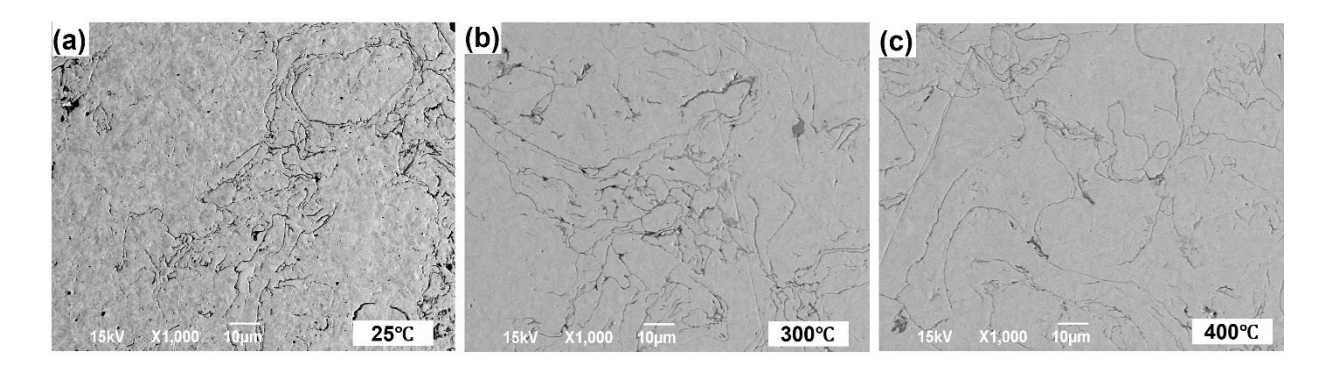


**Figure 4.** Zn coating: Surface SEM images a) at 25°C, and after exposure to b) 300°C, c) 400°C.

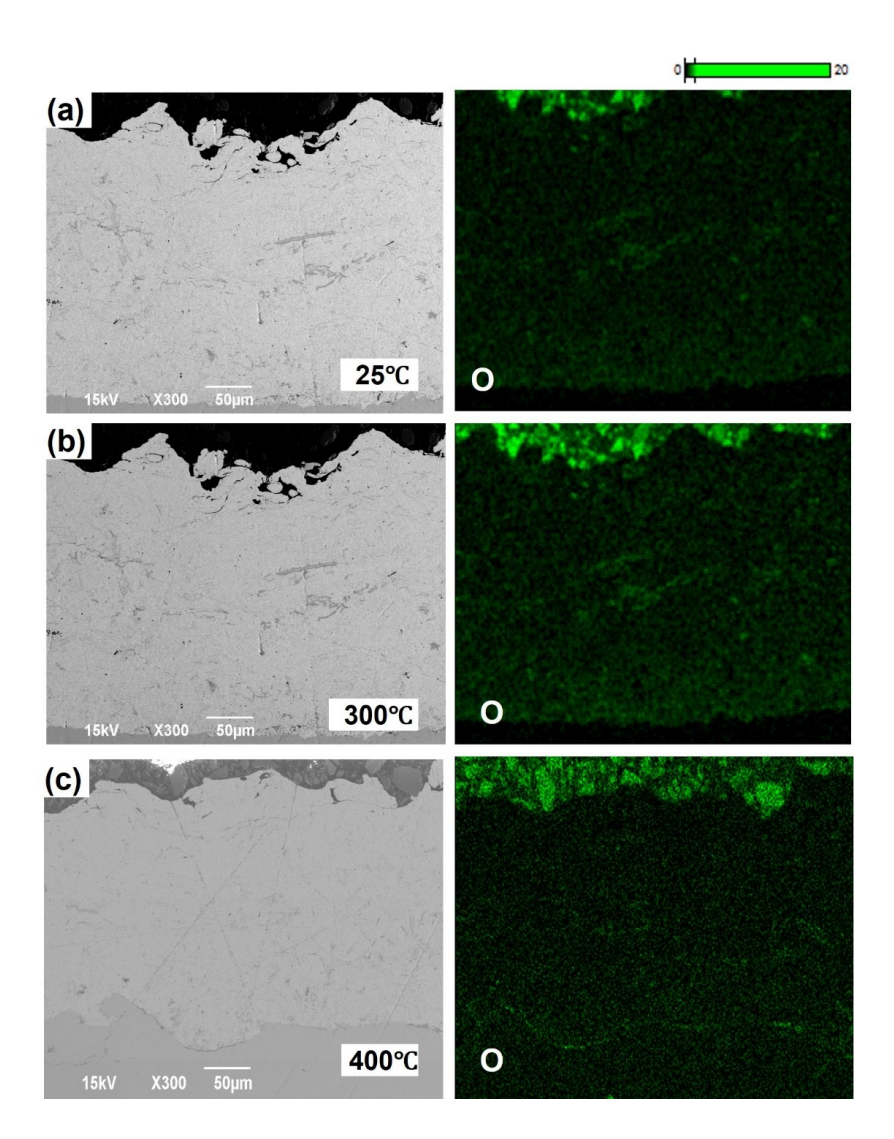


**Figure 5.** Zn coating: Cross-section SEM images a) at 25°C, and after exposure to b) 300°C, c) 400°C, and corresponding EDS maps of oxygen.

The SEM images at 1,000X magnification were taken on the surface of the Al coatings after cooling from exposure temperatures up to 700°C and are shown in Figure 6. The surface micrographs of Al coatings didn't exhibit any signs of damage in the appearance of the microstructure until cooled from 500°C, as depicted in Figures 6 (a) to (d). However, after being cooled from 600°C the coating micrograph showed increased

272

273

274

275276

porosity. Moreover, the surface micrograph of Al coating taken after cooling from 700°C showed the presence of light color phases along with increased porosity as shown in Figure 6 (f). The presence of Fe in EDS mapping of Al at this temperature can be attributed to either the high-temperature oxidation in the coating, possibly resulting in the loss of coating's integrity when exposed to 700°C, or due to the formation of intermetal-lics formed by the Fe which is used as an alloying element in the Al wires. However, examining the corresponding cross-section through an optical microscope revealed a significant reduction in the coating's thickness. This observation indicates that the presence of Fe on the Al surface was likely due to the removal of Al coating thickness during metallographic preparation, which exposed the substrate steel. This is reflected in the micrograph in Figure 6(f) and the EDS map in Figure 6(g). It should also be noted that no further analysis of the possible formation of Fe intermetallics was carried out. In either case, the Al coating's surface micrographs revealed that the deterioration of the microstructure began after exposure to 700°C, despite no noticeable signs of damage being perceived until 800°C exposure in the digital images shown in Figure 2.

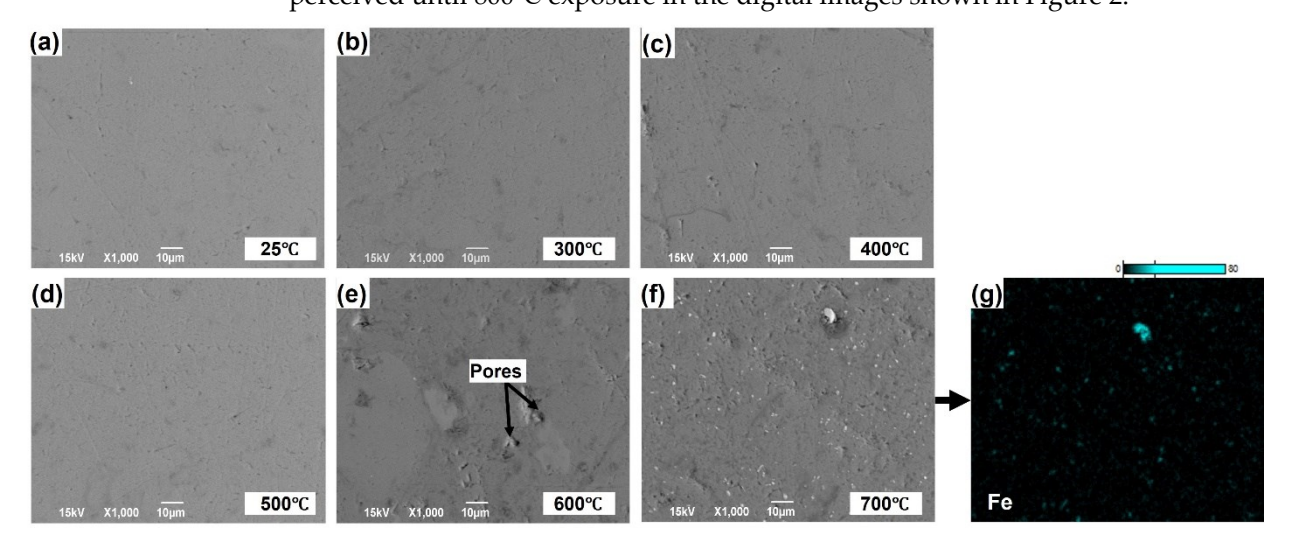


**Figure 6.** Al coating: Surface SEM images a) at 25°C, and after exposure to b) 300°C, c) 400°C, d) 500°C, e) 600°C, f) 700°C, g) EDS map of Fe on Al coating surface after being cooled from 700°C.

The SEM micrographs were captured to gain insights into the microstructural changes on the cross-sections of Al coatings after they had been cooled following exposure to temperatures up to 700°C. Figure 7 displays the SEM images taken on cross-sections of Al coatings and corresponding EDS maps of oxygen after coatings were cooled following the exposure to different temperatures. The changes observed in the cross-section micrographs are in agreement with the observations made from surface micrographs. No obvious signs such as an increase in porosity and through-thickness oxidation were noticed in these micrographs until cooled from 500°C exposure. However, the increased presence of pores and oxidation were apparent in the cross-section micrographs of the Al coatings cooled from 600°C and 700°C (see Figures 7 (e) and (f)). Specifically, the micrograph shown in Figure 7 (f) revealed the presence of a thin sheet of the light grey matrix along the boundary of the Al coating and steel substrate, in addition to the increased oxidation in that region.

314

315

316

317

318

319

320

321

322

323

324

325

326

328

329

330

331

332

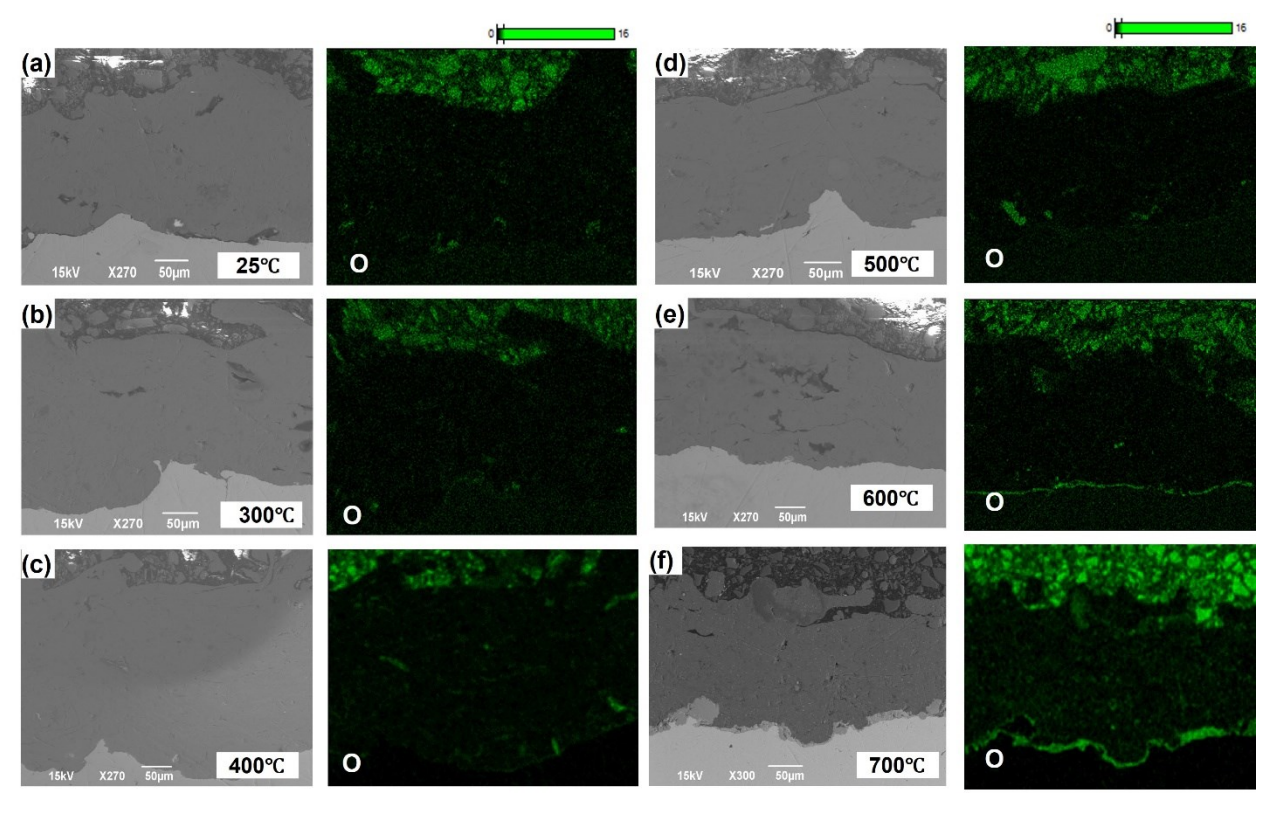
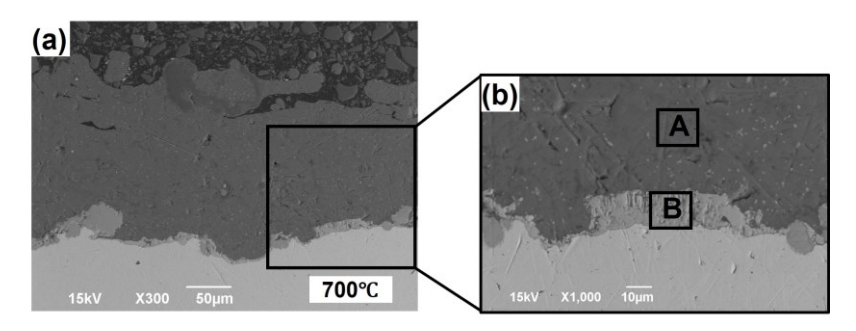


**Figure 7.** Al coating: Cross-section SEM images a) at 25°C, and after b) 300°C, c) 400°C, d) 500°C, e) 600°C, and f) 700°C exposures and corresponding EDS maps of oxygen.

To further investigate these changes, micrographs were taken at a higher magnification of 1000 X on Al coatings after cooling from 700°C and box EDS was performed. Figure 8 shows the results obtained from box EDS analysis conducted at locations near the interface of the coating and the substrate. Figure 8 (b) displays the micrograph of the Al coating at 1000 X magnification and shows the points at which box EDS was performed (points A and B). The elemental composition obtained from EDS analysis is presented in Figure 8 (c). According to the EDS analysis conducted at point A, the primary component of the coating matrix was found to be 87.48 wt.% Al, 5.74 wt.% O, 1.60 wt.% Fe. Whereas, the EDS analysis at point B confirmed that this region was composed of only 0.62 wt.% Al, and 23.86 wt.% O, and 71.94 wt.% Fe, suggesting the possible formation of iron oxide at the coating and substrate interface when exposed to a temperature of 700°C. These changes in the Al coating microstructure at 700°C could have compromised the coating's mechanical integrity leading to excessive removal of the coating's thickness during the metallographic preparation process. This in turn led to the exposure of the substrate steel, as observed in Figure 6 (f). This was further substantiated by the thickness measurements performed using optical microscopy which confirmed the undue removal of the coating.



(c)	Element	AI (Wt.%)	O (Wt.%)	Fe (Wt.%)
	Location			
	Α	87.48	5.74	1.60
	В	0.62	23.86	71.94

**Figure 8.** Cross-section SEM images of Al coating after being cooled from 700°C at a) 300 X magnification b) 1000 X magnification showing the location of box EDS points A, and B c) The composition obtained from EDS performed on points A and B.

The surface micrographs of the Zn-Al pseudo alloy coatings taken at 1000 X magnification after being subjected to different elevated temperatures are shown in Figure 9. As seen in Figures 9 (a) and (b) the Zn-Al pseudo alloy coating microstructure consisted of a light grey matrix corresponding to a Zn-rich area the dark grey region is corresponding to an Al-rich area. The existence of Zn-rich and Al-rich clusters can be explained by the process employed during the deposition of the Zn-Al pseudo alloy coating, which involved the concurrent melting and deposition of individual wires of zinc and aluminum via a wire-arc spray gun. Although distinct and more independent clusters of Zn-rich and Al-rich regions were clearly visible until cooled from a temperature of 300°C, the melting and rearrangement of the constituent metals had taken place beyond this temperature.

Figure 9 (c) shows the surface micrograph of the Zn-Al pseudo alloy coating after cooling from 400°C, and it didn't exhibit a clear distinction between the Zn-rich and Alrich regions. Specifically, following the cooling from 500°C, the coating microstructure revealed the formation of new metallurgical phases. While visible at 1,000X magnification, micrographs at higher magnification (2,500X) were taken to confirm the microstructural arrangement of the new phases, and the EDS analysis for the elemental composition was performed, and the three new phases are clearly visible in 2500 X magnification image shown in Figure 9 (d). As marked the three phases were found to be the eutectoid  $(\alpha+\eta)$  (composition: 78 wt.% Zn, and 22 wt.% Al), partially converted eutectic  $(\beta+\eta)$ ((composition: 89 wt.% Zn, and 11 wt.% Al), and η phase (zinc-rich). Since Zn-Al pseudo alloy coatings were not produced from a pre-alloyed wire, the standard phase diagrams applicable for Zn-Al alloys are not directly applicable in this case, and therefore these phases were confirmed from the existing literature. Interestingly, a similar phase transformation occurred in wire-arc sprayed Zn-15Al alloy coatings produced from prealloyed wires, which were subjected to a temperature of 500°C [19]. The results obtained from the EDS analysis were also consistent with previous reports in the literature [29, 30]. The SEM image taken at 2,500 X revealed the microstructural arrangement of these phases where in a lighter matrix of η phase, the peanut-shaped lamellar structure of the eutectoid ( $\alpha$ + $\eta$ ) phase was present, and a coarse lamellar structure of the eutectic ( $\beta$  +  $\eta$ ) surrounding it. These microstructural changes observed were comparable to those re333 334

335

336

337

> > 359

360

361

362

363

365

366

369

ported in previous studies that utilized Zn-Al alloys as lead-free high-temperature solders [29].

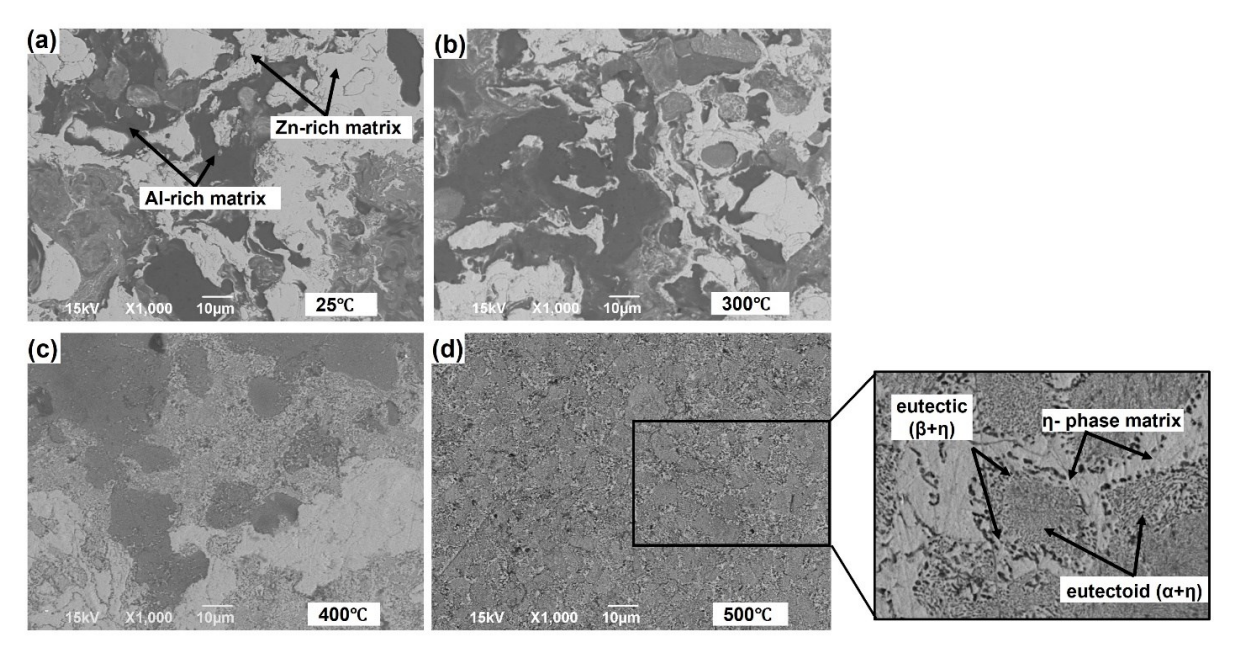


**Figure 9.** Zn-Al pseudo alloy coating: Surface SEM images a) at 25°C, and after exposure to b) 300°C, c) 400°C, and d) 500°C.

In Figure 10, the cross-sectional SEM micrographs of the Zn-Al pseudo alloy coatings following cooling from exposure to high temperatures are presented, accompanied by the elemental maps of oxygen, zinc, and aluminum. Despite the fact that these crosssection micrographs do not readily show phase changes at the magnification used, a rise in porosity was observed as the exposure temperature increased (see Figures 10 (a) to (d)). The cross-section micrographs displayed alternating lamellar structure of Zn-rich and Al-rich areas till an evelated temperature of 300°C. However, the microstructure of the cross-section micrographs corresponding to 400°C and 500 °C exhibited a more uniform distribution of zinc and aluminum compared to its as-deposited conditions which can also be noticed in the corresponding EDS maps of zinc and aluminum presented in Figure 10. Moreover, the EDS maps of oxygen indicated a substantial rise in oxygen content as the exposure temperature increased. The alterations in the coating's microstructure, including the appearance of new phases, and restructuring of zinc and aluminumrich regions, the escalation of porosity, and high-temperature oxidation, which were observed from SEM and EDS analysis of the Zn-Al pseudo alloy coatings, conceivably resulted in the failure of the coating beyond an exposure temperature of 500°C, evidenced by surface cracking shown in Figure 3 (e).

370

371 372

373

387

388

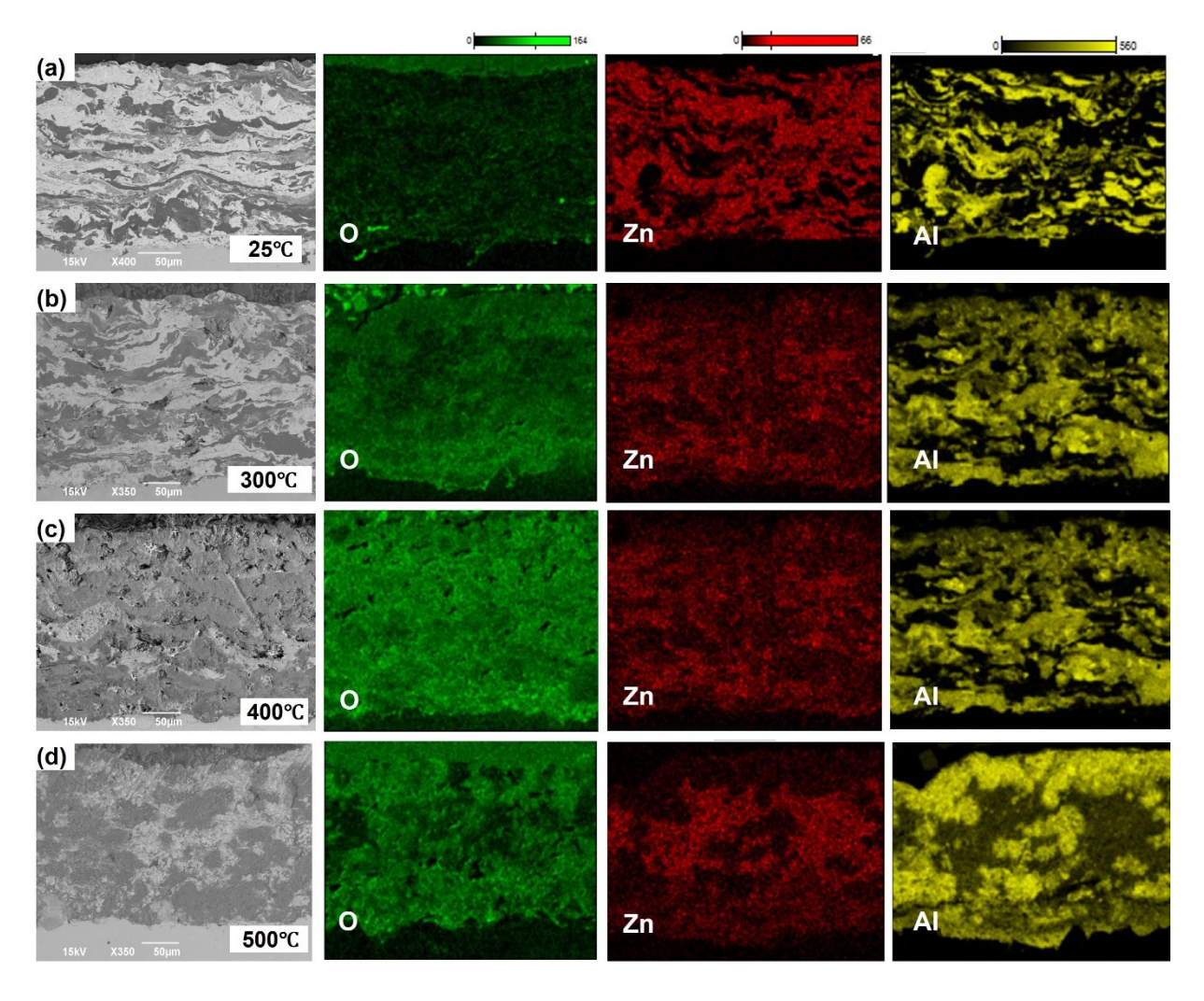


**Figure 10.** Zn-Al pseudo alloy coating: Cross-sectional SEM images s with corresponding EDS maps of elements oxygen, zinc, and aluminum a) at  $25^{\circ}$ C, and after exposure to b)  $300^{\circ}$ C, c)  $400^{\circ}$ C, d)  $500^{\circ}$ C.

#### X-ray Diffraction Analysis

The metallurgical phases present in pure Zn, pure Al, and Zn-Al pseudo alloy coatings were identified by performing XRD characterization after cooling from different elevated temperatures. Figure 11 presents the XRD patterns obtained from the surface of as-deposited Zn coating, as well as from the Zn coatings cooling from 300°C and 400°C exposure. The XRD pattern was found to be similar for all three exposure conditions, with peaks indicating the presence of pure zinc and fewer weak peaks corresponding to the presence of zincite (ZnO). The presence of ZnO in the as-deposited conditions can be attributed to the oxidation of liquid metal droplets during the coating deposition process, as well as oxidation during the necessary polishing process performed to minimize X-ray pattern noise, as Zn is highly reactive and quickly oxidizes [31]. Additionally, exposure to high temperatures of 300°C, and 400°C might have resulted in the formation of ZnO in these coating specimens, and hence detected by the XRD instrument. Figure 12 (a) shows XRD patterns of Al coatings obtained in their un-exposed conditions and after 300°C and 400°C exposures. Pure aluminum was the only distinguishable phase in all three temperature conditions. Figure 12 (b) presents the diffraction peaks generated from Al coatings after cooling from exposure to 500°C, 600°C, and 700°C. The Al coating cooled from 500°C revealed peaks of pure aluminum only, similar to the pattern observed in Figure 12 (a).

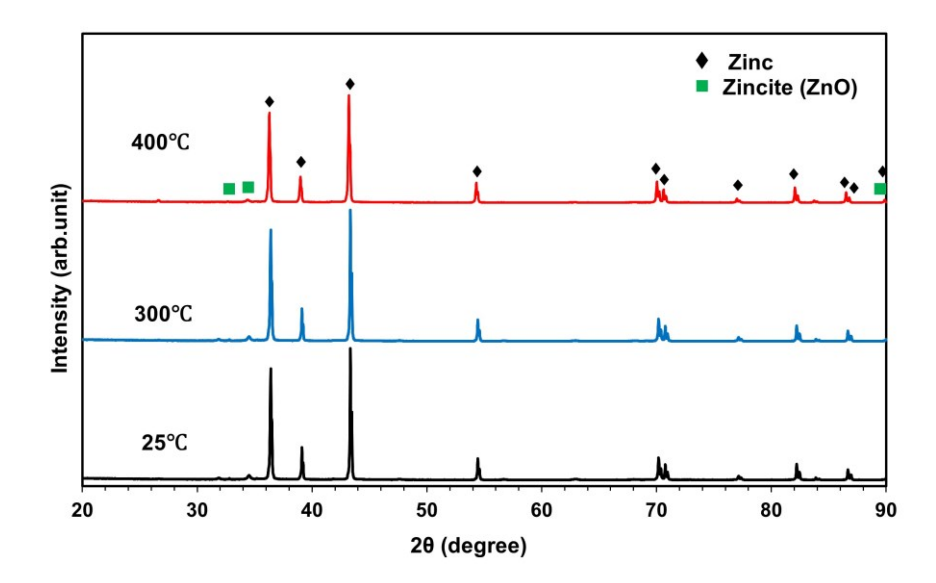
390

391

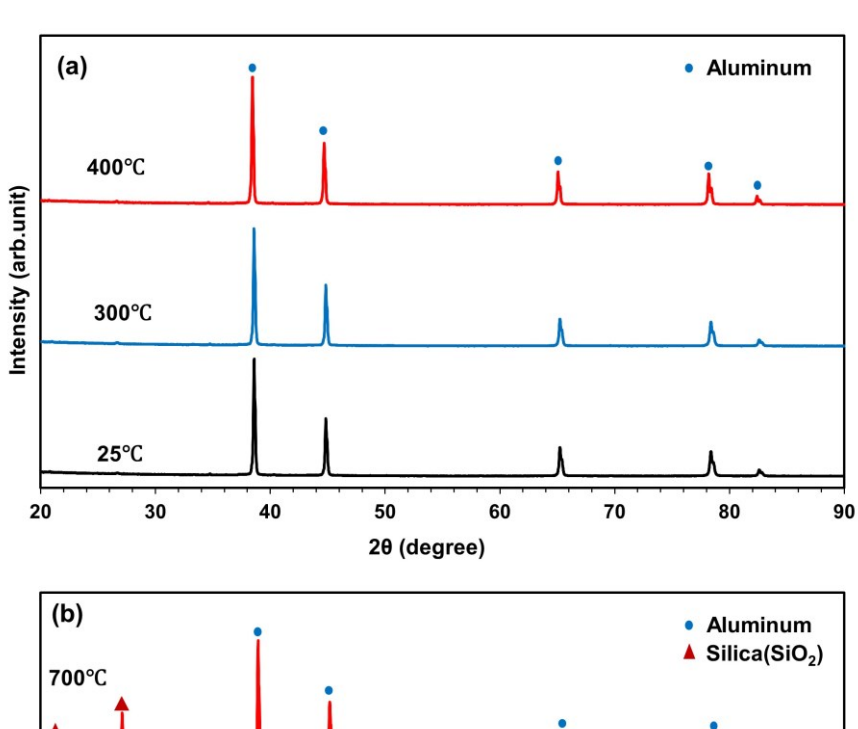
392 393

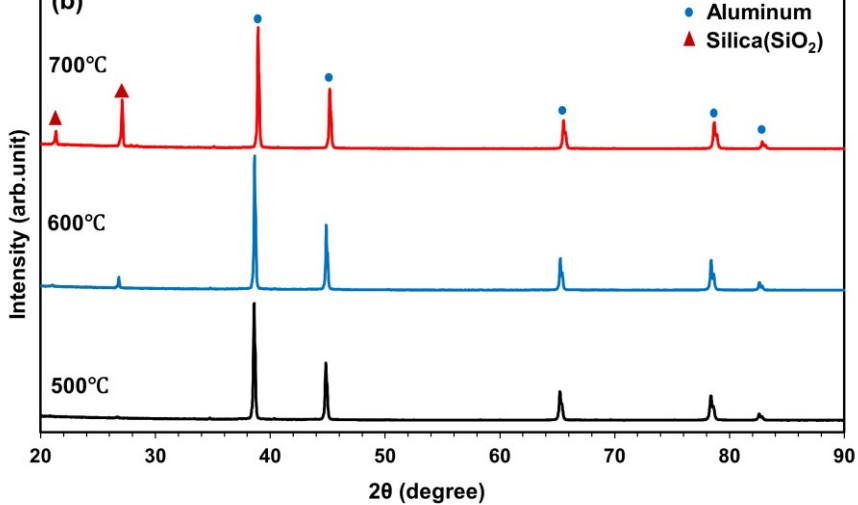
394 395

412



**Figure 11.** XRD patterns from Zn coatings at 25°C and after exposure to 300°C, and 400°C.

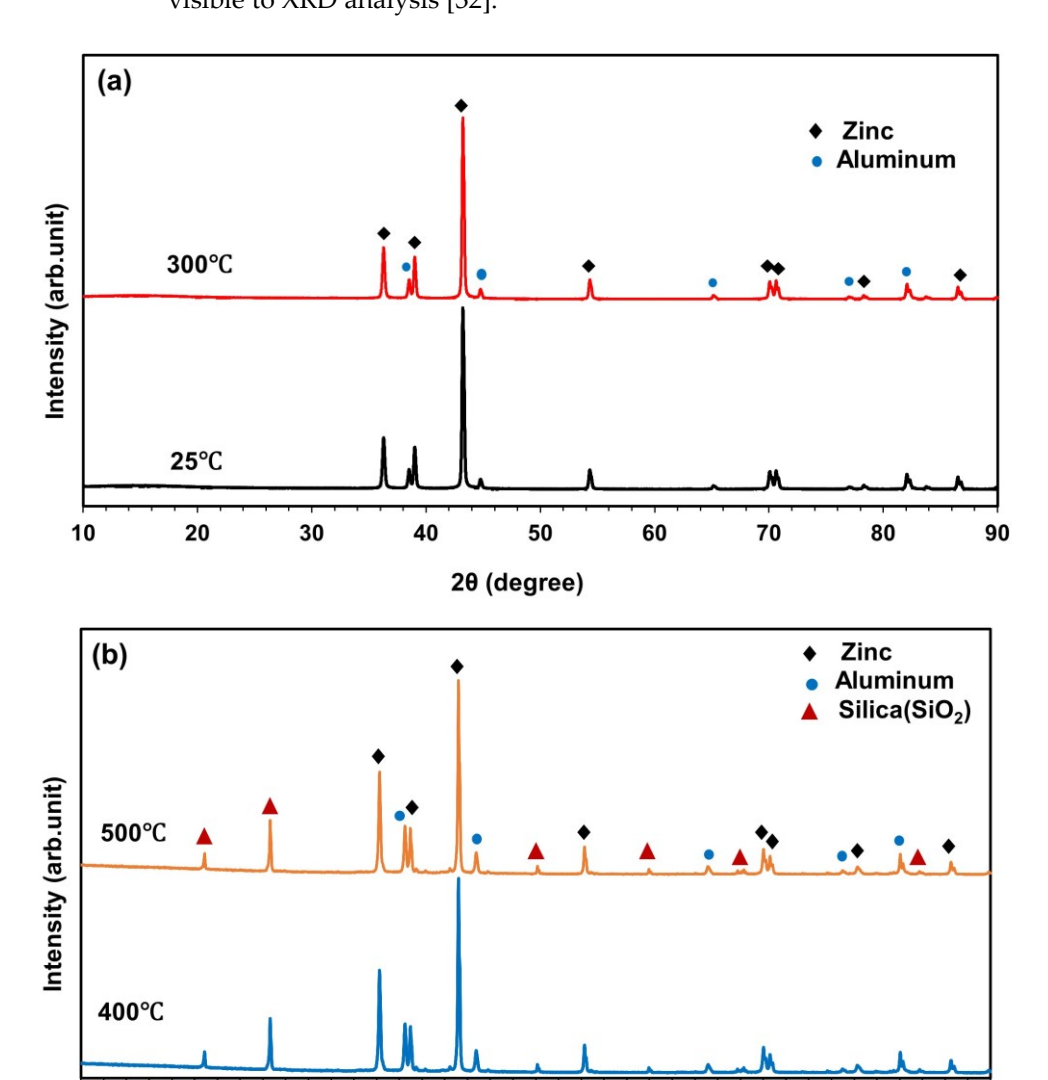




2θ (degree)

**Figure 12.** XRD pattern from Al coatings a) at 25°C and after exposure to 300°C and 400°C, and b) after exposure to 500°C, 600°C, and 700°C.

In Figure 13 (a), the XRD patterns of the Zn-Al pseudo alloy coating before exposure to high temperatures and after exposure to 300°C, while Figure 13 (b) shows the diffraction peaks after cooling from 400°C and 500°C exposures. The XRD patterns of the pseudo alloy coating remained unchanged before and after exposure to 300°C, comprising peaks of zinc and aluminum only. Similarly, XRD spectra of Zn-Al pseudo alloy coating cooled from 400°C, and 500°C showed peaks characteristic of zinc and aluminum, mirroring those observed in the as-deposited condition seen in Figure 13 (a). However, additional peaks corresponding to silica were observed in these coatings, which may have arisen from the retention of silica in the microstructure of the Zn-Al pseudo alloy coating that exhibited a higher degree of porosity after exposure to 400°C, and 500°C as noticed in Figures 10 (c) and (d). Although the formation of zinc, and aluminum oxidation products was expected, no corresponding peaks were detected in the XRD spectra of the coating after 400°C, and 500°C exposures. This suggests that the formed oxide films on the surface of the coating may exist in an amorphous state, rendering them invisible to XRD analysis [32].



436

437

438

439

440

441

442

443

445

446

447

448

449

450

451

452

453

454

455

456

457

459

**Figure 13.** XRD pattern from Zn-Al pseudo alloy coatings a) at 25°C and after exposure to 300°C, and b) after exposure to 400°C and 500°C.

# Microhardness and Porosity Analyses

Figures 14, 15, and 16 present the plots depicting the variation in microhardness and porosity versus the exposed target elevated temperatures for Zn, Al, and Zn-Al pseudo alloy coatings respectively. Figure 14 illustrates that the average Vickers microhardness values for the Zn coatings showed a trend of increasing magnitude with higher exposure temperatures. The average microhardness of the Zn increases as the temperature increases till 400°C. Furthermore, Figure 14 reveals a decrease in the average porosity percentage as the exposure temperature increases. The values of microhardness and porosity of the as-deposited Zn coatings are consistent with those previously documented in the literature [33]. The observed increase in microhardness and decrease in porosity as the exposure temperature increased can be attributed to the melting and rearrangement of the Zn coating microstructure at higher temperatures. The surface and cross-section micrographs of Zn coatings presented in Figures 4 and 5 also demonstrated the reduction in the number of pores, irregularities, and splat boundaries in the coating microstructure after cooling from 300°C and 400°C compared to its as-deposited samples. The microhardness and porosity results for Zn coatings indicate that the exposure to higher temperatures led to an improved coating microstructure, likely due to the heattreatment effect caused by high-temperature exposure. The heat treatment process is a widely used post-treatment process where metals, alloys, and coatings are exposed to high temperatures for a fixed duration to reduce the interconnected porosity and intersplat boundaries and to improve the microstructure [34]. These findings are consistent with previous studies that have demonstrated the benefits of heat treatment in enhancing the properties of coatings and other materials [35].

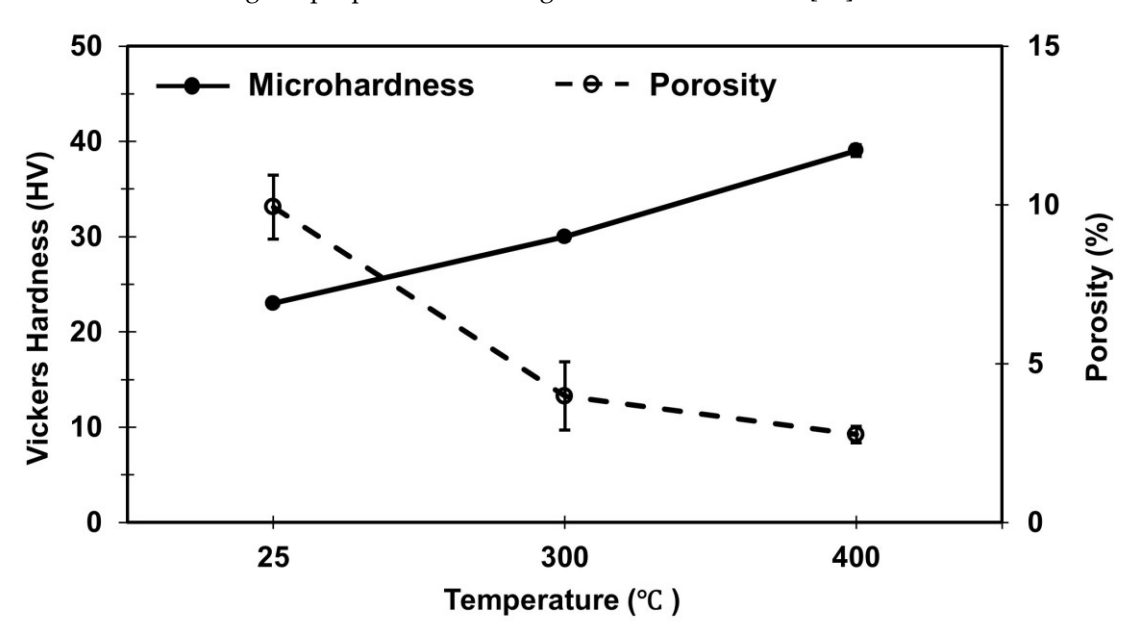


Figure 14. Vickers microhardness and porosity vs temperature plot of pure Zn coatings.

Figure 15 displays the changes in average microhardness and porosity values for Al coating as it was exposed to different target elevated temperatures. The graph shows that the average microhardness of the Al coatings increased with an increase in exposed temperature up to 400°C, and then displayed a decreasing trend from 500°C to 700°C. Although the average microhardness corresponding to 500°C was less than the value calculated from 400°C exposed coating, the value was still higher than the hardness val-

460

461

462

463

465

466

ue obtained from the Al coating in the as-deposited condition. However, the microhardness values for Al coatings cooled from 600°C and 700°C exposure was much lower than those for Al coatings at 25°C and can be considered as an actual decrease in microhardness at these temperatures. The average microhardness values obtained for Al coatings were as follows: 42 HV, 45 HV, 54 HV, 46 HV, 36 HV, and 35 HV at 25°C and after cooling from 300°C, 400°C, 500°C, 600°C, and 700°C, respectively. The microhardness values obtained from as-deposited Al coatings are in agreement with the values documented in existing literature [36]. The porosity values, on the other hand, showed a slight decrease after 300°C exposure and stayed consistent up to 500°C, followed by an increasing trend from 500°C to 700°C. The actual porosity percentages were below 10% until 600°C and it increased to 13% after exposure to 700°C. The improved microhardness and decreased porosity values up to 500°C can be attributed to the heat treatment effect discussed before, which caused positive changes in the Al coatings' microstructure. However, the decrease in microhardness and increased porosity at 600°C and 700°C can be attributed to the escalated oxidation at elevated temperatures, which deteriorated the microstructure around and beyond the melting point (660°C) of Al. The results of microhardness and porosity are consistent with the observations drawn from SEM images shown in Figures 6 and 7 where the changes in porosity and oxidation are noticeable.

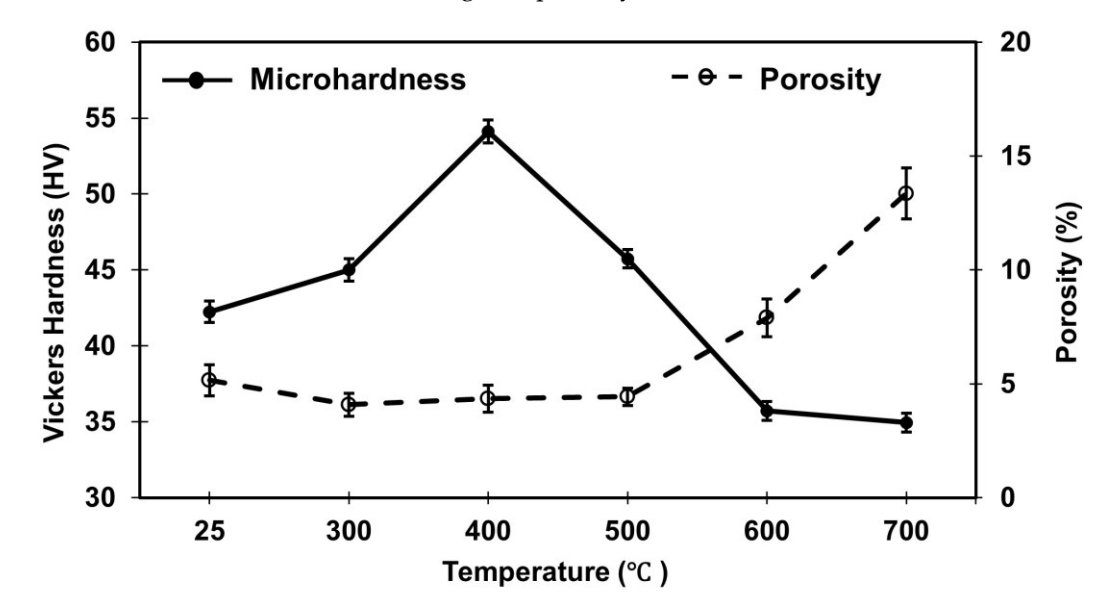


Figure 15. Vickers microhardness and porosity vs temperature plot of pure Al coatings.

Figure 16 shows the graph between microhardness and porosity versus temperature for Zn-Al pseudo alloy coatings. The average microhardness values increased consistently with an increase in temperature from 25°C to 500°C, which can be due to the conversion of the coating into a nanocrystalline form from its amorphous state [35]. Additionally, the formation of brittle intermetallic phases such as eutectic ( $\eta$ +  $\beta$ ), eutectoid ( $\alpha$ + $\eta$ ), and  $\eta$  which can be seen from SEM images shown in Figure 9 would also contribute to the increased hardness of the coating. On the other hand, the porosity values increased from 3% at 25°C to 20% after exposure to 500°C. This increase in porosity is contrary to what was observed in pure Zn, and pure Al coatings which showed decreased porosity values until 400°C exposure and 500°C exposure respectively. The porosity rise observed in Zn-Al pseudo alloy coating after cooling from elevated temperature exposures can be ascribed to both the thermal incompatibility between the Zn and Al and escalated thermal oxidation in the coating microstructure. The increased porosity and increased oxidation are clearly seen in cross-section micrographs shown in Figure 10 and the results of microhardness and porosity agree with SEM and EDS analysis results.

504

505

506

507

508

509

510

511

512

513

514

515

516

517

518

519

520

521

522

523

524

525

526

527

528

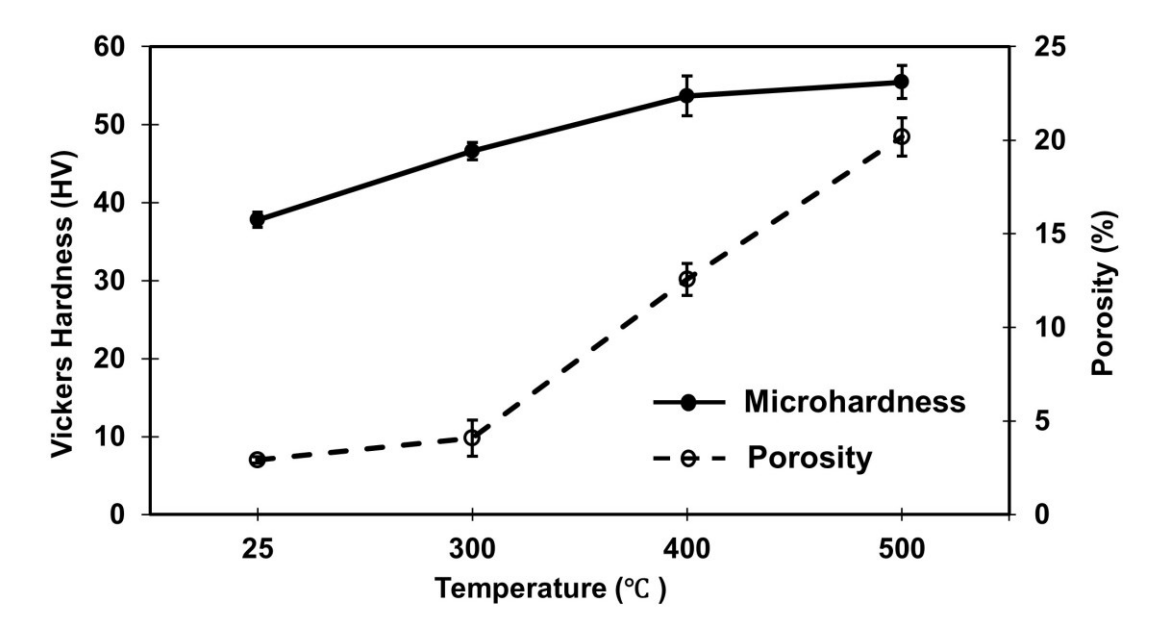


**Figure 16.** Vickers microhardness and porosity vs temperature plot of Zn-Al pseudo alloy coatings.

#### Abrasion resistance

The bar plot shown in Figure 17 presents the results of the sandpaper abrasion test performed on Zn, Al, and Zn-Al pseudo alloy coatings. The abrasion loss for Zn coatings was nominal, staying under 4% in un-exposed conditions, and remained consistent even after exposure to elevated temperatures of 300°C and 400°C. These findings align with the outcomes of all the previous tests performed for characterization, including SEM and EDS analyses, microhardness, and porosity tests, which indicated that the Zn coatings' integrity remained intact following exposure to target high temperatures reaching up to 400°C. Al coatings displayed varying abrasion loss ranging from 7% to 9% in their as-deposited conditions and until being cooled from 500°C exposure. Upon cooling from 600°C, the abrasion loss for Al coatings increased to 13%, and a significant increase in abrasion/wear loss of approximately 50% was observed after cooling from 700°C exposure. This increase in abrasion loss can be ascribed to the occurrence of elevated thermal oxidation, which leads to the formation of Al oxidation products that are vulnerable to wear/abrasion and compromised the coating's mechanical integrity. The results of the abrasion test of Al coatings align with the surface SEM image of Al coating after 700°C exposure seen in Figure 6 (f) which indicated the steel substrate exposed after cooling from 700°C, as well as the cross-sectional SEM image, and the EDS map of oxygen presented in Figure 7 (f), which further elucidates the heightened oxidation within the microstructure of the coating. Although the Al coating cooled from 700°C didn't exhibit fragile-to-touch behavior, the results from microhardness, porosity, and abrasion tests suggest a deterioration and loss of mechanical integrity in the Al coating after exposure to 700°C.

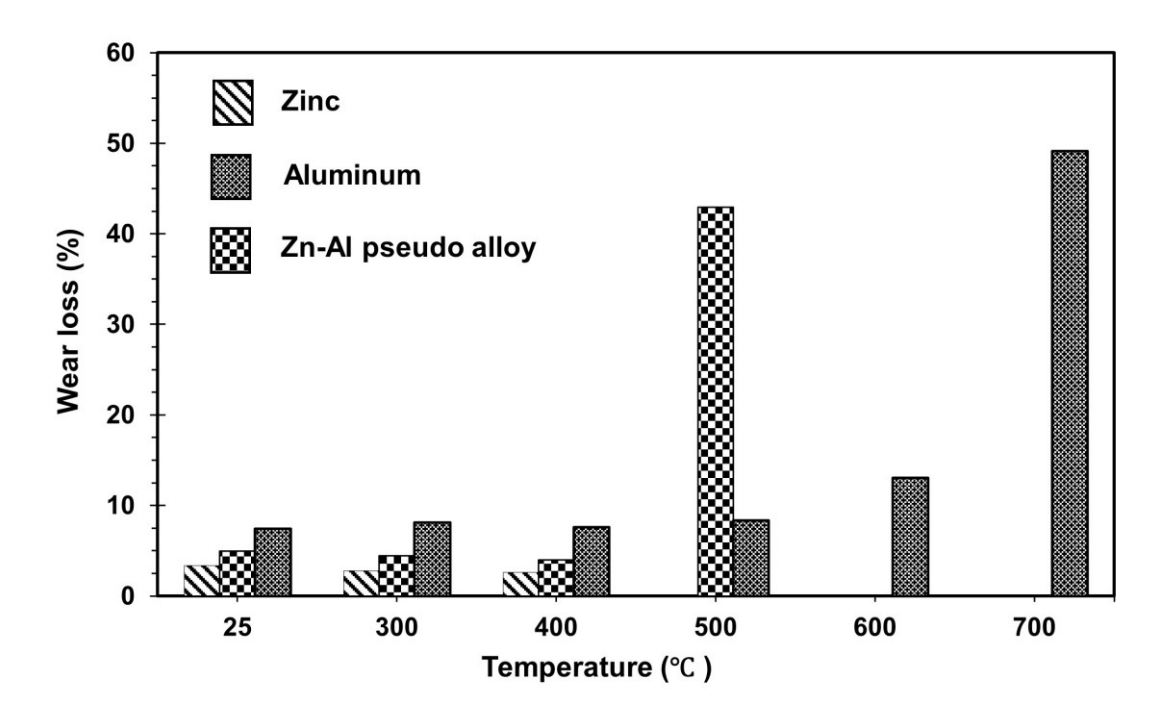


Figure 17. Percentage wear/abrasion loss of the coatings versus exposure temperature.

The abrasion test results of Zn-Al pseudo alloy coating indicated an abrasion loss of under 5% in their as-deposited conditions and for coatings subjected to temperatures up to 400°C. However, samples that were cooled from 500°C exhibited a significant increase in abrasion loss of approximately 43%. As can be observed in the SEM images as seen in Figure 9 (d), the formation of brittle intermetallic phases and the formation of high-temperature oxidation products of Zn and Al could have made the Zn-Al coating's microstructure fragile and susceptible to abrasion after exposure to 500°C.

# **Electrochemical Impedance Spectroscopy**

The electrochemical impedance spectroscopy was carried out to determine the variations in the electrochemical corrosion behavior of the Zn, Al, and Zn-Al pseudo alloy coatings after high-temperature exposures when compared to their as-deposited conditions. The EIS data called the Bode plot, a graph between frequency and modulus of impedance, is used [43] to investigate the corrosion resistence in Figure 18 for Zn coating. According to the Bode modulus plot, the impedance values of Zn coating were as follows: 147  $\Omega$ -cm² in un-exposed conditions, 157  $\Omega$ -cm² after cooling from 300°C, and 253  $\Omega$ -cm² after cooling from 400°C exposure. This indicates the Zn coating surface has exhibited a slightly improved resistance to corrosive media after exposure to elevated temperatures due to the improved microstructure and the presence of high-temperature oxidation products discussed previously, which restricted the movement of ions [37-42].

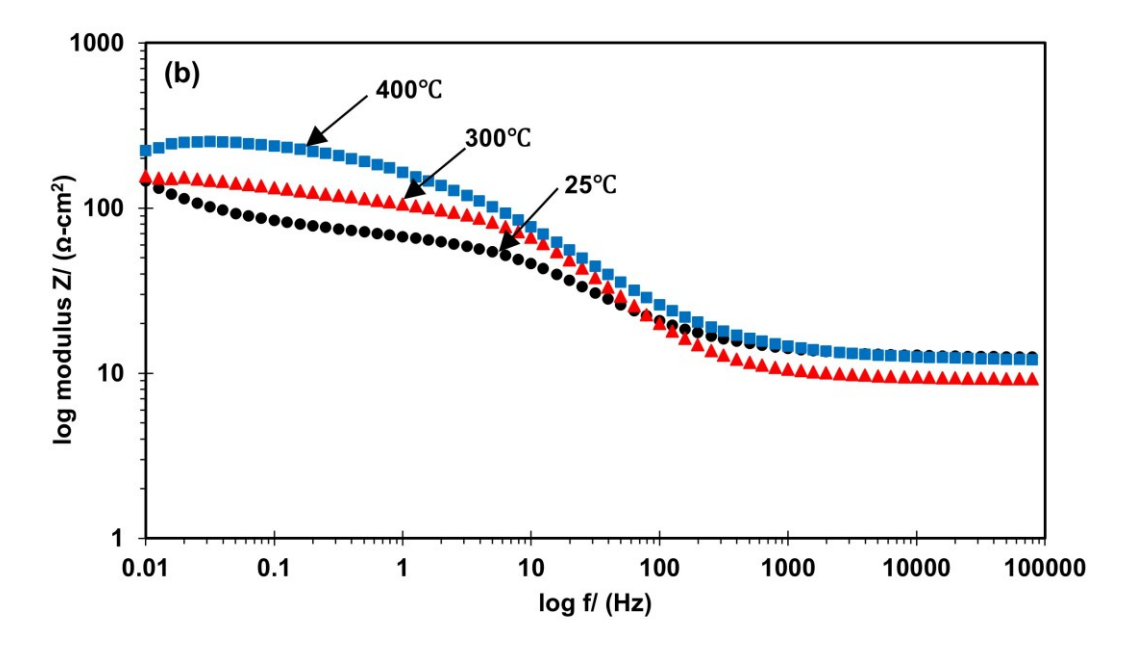


Figure 18. Bode-modulus plots for Zn coatings at 25°C and after exposure to 300°C, 400°C.

In addition to the physical interpretation of the data, the EIS also allows us to represent the data into an equivalent electrical circuit (EEC), which helps us understand the coatings' corrosion mechanisms. Accordingly, the developed EECs of the three sets of coatings are presented in Figure 19. The EIS data from un-exposed Zn coating (25°C), and Zn coating after exposure to 300°C can be best represented using a Randles circuit with Warburg element as shown in Figure 19(a). This circuit consisted of the following elements: Rs, which pertains to the solution resistance, CPEdI denotes the double-layer capacitance, Rct represents the charge transfer resistance of the coating, and W is the Warburg impedance which accounts for the diffusion processes [44] discussed before. On the other hand, the EEC for the Zn coating after exposure to 400°C consisted of additional circuit elements including Rf and CPEf representing the resistance and constant phase element offered by the corrosion/oxidation product layer formed on the coating's surface. Moreover, the low-frequency Warburg impedance observed earlier was transformed into an inductive loop after 400°C exposure. This behavior was modeled in EEC with two elements R<sub>L</sub> and L which represent the inductance resistance and inductance respectively indicating the adsorbed layer [45] as discussed above.

552 553

554

555

556

557

558

559

560

561

562

563

565

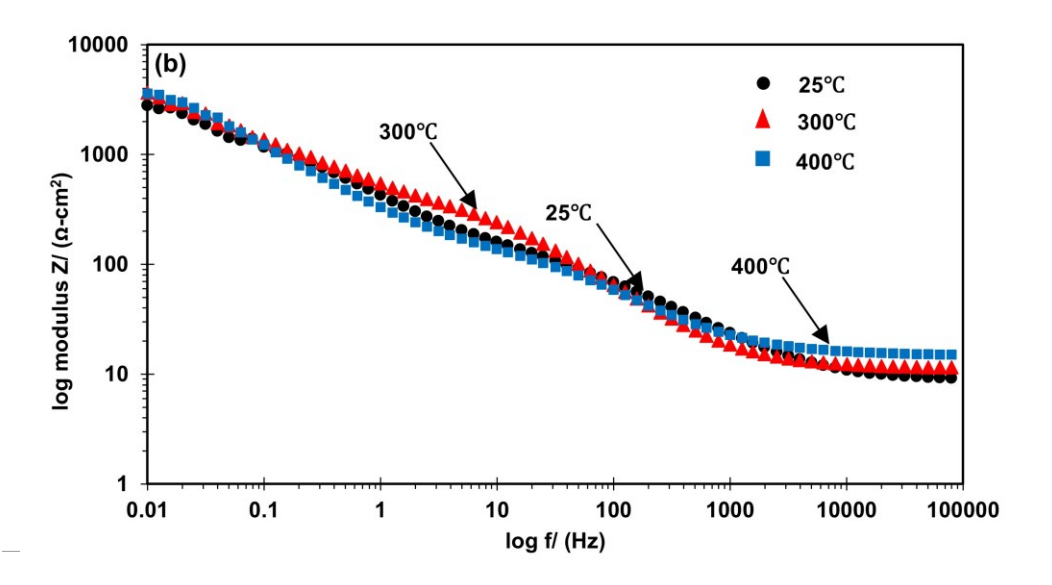
566

567

568

**Figure 19.** (a) Equivalent circuit model for (a) Zn coating at 25°C and after 300°C exposure, (b) Zn coating after 400°C exposure, (c) Al coatings and Zn-Al pseudo alloy coatings.

The actual changes in impedance values for Al coating after cooling from exposure temperatures up to 400°C are shown in the Bode modulus plot presented in Figure 20. For exposure temperatures ranging from 500°C to 700°C, the impedance values can be seen in the Bode modulus plot shown in Figure 21. According to the Bode modulus frequency plots, the impedance values of Al coating at 25°C, and after cooling from 300°C, 400°C, 500°C, 600°C, and 700°C were 2787  $\Omega$ -cm², 3602  $\Omega$ -cm², 3665  $\Omega$ -cm², 2833  $\Omega$ -cm², 2195  $\Omega$ -cm², 1814  $\Omega$ -cm² respectively. The impedance values of Al coating after cooling from 600°C, and 700°C were lower than the impedance values obtained in asdeposited conditions suggesting a decrease in the corrosion protection performance of the coating after being exposed to these temperatures [45]. Although the impedance values indicate the potential corrosion protection from Al coating even after being subjected to 700°C, it is recommended to replace them due to the loss of mechanical integrity of the Al coating at this temperature as discussed in the previous sections.



570

571

572

573

574

575

576

577

578

579

580

581

582

583

584

**Figure 20.** Bode-modulus plots for Al coating at 25°C and after cooling from 300°C, 400°C exposures.

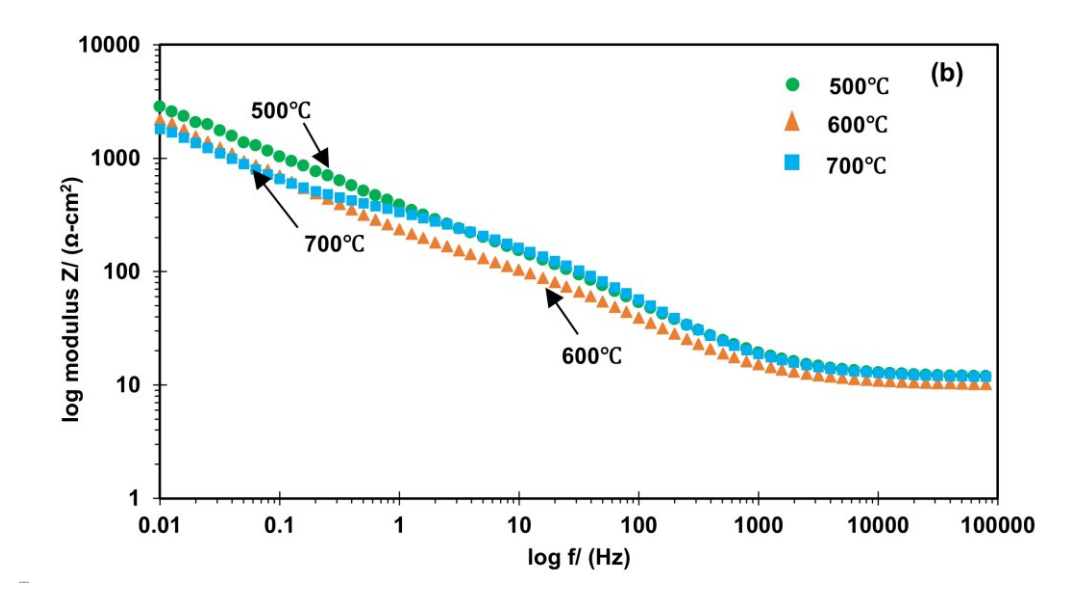


**Figure 21** Bode-modulus plots for Al coating after cooling from 500°C, 600°C, and 700°C exposures.

The EEC that best represents the behavior of both Al coatings and Zn-Al pseudo alloy coatings after being subjected to various elevated temperatures is shown in Figure 19 (c). The EEC consisted of Rs (CPE<sub>f</sub>, and R<sub>f</sub>) (CPE<sub>dl</sub>, and R<sub>ct</sub>) elements, where CPE<sub>f</sub> and R<sub>f</sub> represent the constant phase element and resistance corresponding to the corrosion product or passivation layer formed on the surface of the coating and CPE<sub>dl</sub> and R<sub>ct</sub> refers to the constant phase element for the double layer capacitance (between coating and electrolyte), and charge transfer resistance of the coating respectively and finally, R<sub>s</sub> refers to the solution resistance [46] as mentioned already.

The Bode modulus plot of Zn-Al pseudo alloy coatings is presented in Figures 22. The impedance values obtained from the Bode modulus plot at 25°C, and after cooling from 300°C, 400°C, and 500°C were 281  $\Omega$ -cm<sup>2</sup>, 645  $\Omega$ -cm<sup>2</sup>, 1620  $\Omega$ -cm<sup>2</sup>, and 1247  $\Omega$ -cm<sup>2</sup> respectively. This trend indicates an improvement in the coating's corrosion resistance with an increase in exposure temperature, and this can be attributed to the formation of intermetallic phases, rearrangement occurred in the coating's microstructure due to the melting of the constituent metals at high temperatures, in addition to the oxidation products formed at high temperatures as discussed earlier. The increased porosity observed in Zn-Al pseudo alloy coatings after subjecting them to 500°C didn't affect the EIS results much. This could be either due to the larger surface area of the porous coating which could have facilitated the deposition of oxidation products on more active sites, effectively obstructing the passage of corrosive medium into the coating or the existence of spherical-shaped pores which were not linked to the coating's top surface hence didn't show a negative impact on the coating's electrochemical behavior [46-48]. However, with the observed increase in porosity, reduced hardness, and increased wear loss it is recommended to replace Zn-Al pseudo alloy coatings that are subjected to temperatures 500°C and beyond.

590

591 592

603

604

615

616

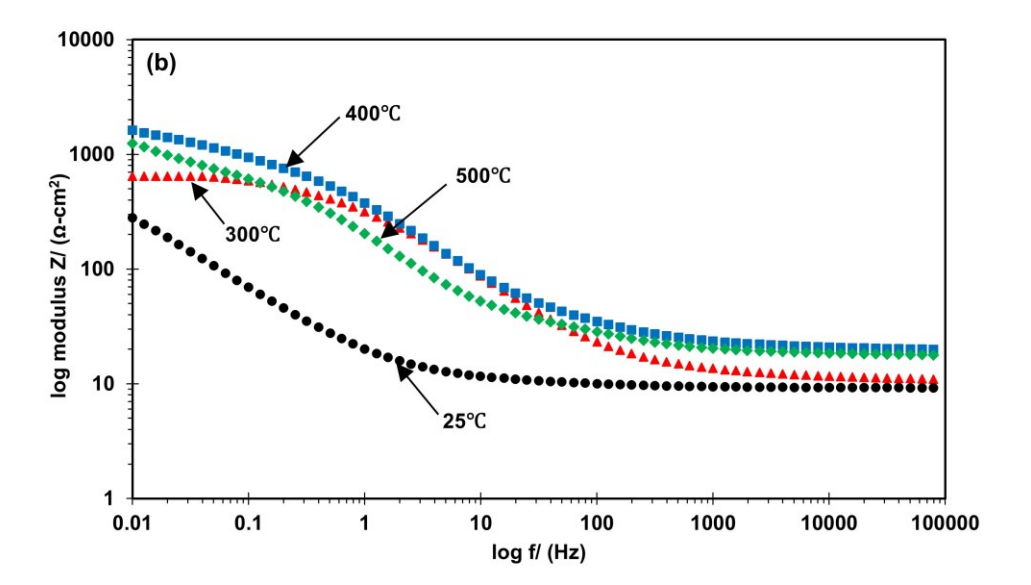


**Figure 22** Bode-modulus plots for Zn-Al pseudo alloy coating at 25°C and after cooling from 300°C, and 400°C exposures.

Conclusions

The study provides a comprehensive analysis of the performance of Zn, Al, and Zn-Al pseudo alloy coatings produced through wire-arc spraying, following exposure to high fire temperatures. The primary focus of this investigation is to examine the alterations in the coatings' microstructure, mechanical integrity, and electrochemical behavior based on the temperature of exposure. The study draws the following conclusions:

- (1) Exposing Zn coatings to temperatures up to 400°C had a beneficial effect on their overall performance.
- (2) The Al coatings showed relatively unchanged coating performances when exposed to temperatures up to 500°C when compared to the original condition. A slight decline in the desirable properties was noticed after exposure to 600°C. However, after being subjected to 700°C the coating exhibited a substantial decrease in its protection performance.
- (3) The Zn-Al pseudo alloy coatings formed brittle intermetallic phases after exposure at 500°C. The desirable properties of the Zn-Al pseudo alloy coating remained intact up to 400°C exposure. After cooling from 500°C, athough still intacted, a substantial increase in the coating's porosity and higher susceptibility to abrasion was noticed in the coating.

In summary, the Zn and Zn-Al pseudo alloy coatings showed an improved or unaffected protection performance up to 400°C while Al coatings remained affected up to 500°C, but were slightly compromised when exposed to 600°C, and deteriorated when subjected to 700°C. However, it is recommended to properly seal the fire-exposed Zn, Al, and Zn-Al pseudo alloy coatings prior to their reuse to address the coatings' porosity and to increase their service life and corrosion protection performance. In the Future, full-scale testing of this wire-arc sprayed steel components can be performed to verify the findings of the small-scale tests under ISO fire scenario conditions. In addition, the influence of convection in the furnace and radiation from walls and ceiling on the results can also be researched.

**Author Contributions: Ratna Yasoda**: Data curation, Methodology, Formal analysis, Investigation, Writing - original draft, Writing - review & editing. **Nour Hakim**: Formal analysis, Investigation,

tion **Ying Huang:** Project administration, Funding acquisition, Methodology, Supervision, Writing - review & editing. **Xiaoning Qi:** Investigation, Writing - review & editing.

**Acknowledgments:** This work was supported by the National Science Foundation under Grant No. CMMI-1750316 and OIA-2119691. The findings and opinions expressed in this article are those of the authors only and do not necessarily reflect the views of the sponsors.

#### References

- 1. S. Brito, I. Bastos, H. Costa, Corrosion resistance and characterization of metallic coatings deposited by thermal spray on carbon steel, *Materials & Design*, **41**, 282-288 (2012) 660
- 2. P.L. Fauchais, J.V. Heberlein, M.I. Boulos, Thermal spray fundamentals: from powder to part, Springer Science & Business Media, 2014
- 3. H. Katayama, S. Kuroda, Long-term atmospheric corrosion properties of thermally sprayed Zn, Al and Zn–Al coatings exposed in a coastal area, *Corrosion Science*, **76**, 35-41 (2013)
- 4. R.D. Yasoda, Y. Huang, X. Qi, Corrosion Performance of Wire Arc Deposited Zinc Aluminum Pseudo Alloy and Zinc 15 Aluminum Alloy Coatings on Steel in Chloride Environment, *Journal of Thermal Spray Technology*, 1-16 (2022)
- 5. T.-Y. Yung, T.-C. Chen, K.-C. Tsai, W.-F. Lu, J.-Y. Huang, T.-Y. Liu, Thermal spray coatings of Al, ZnAl and inconel 625 alloys on SS304L for anti-saline corrosion, *Coatings*, **9**(1), 32 (2019)
- 6. M. Garlock, I. Paya-Zaforteza, V. Kodur, L. Gu, Fire hazard in bridges: Review, assessment and repair strategies, *Engineering structures*, **35**, 89-98 (2012)
- 7. X. Li, F. Khan, M. Yang, C. Chen, G. Chen, Risk assessment of offshore fire accidents caused by subsea gas release, *Applied Ocean Research*, **115**, 102828 (2021)
- 8. C. Lam, W. Zhou, Statistical analyses of incidents on onshore gas transmission pipelines based on PHMSA database, *International Journal of Pressure Vessels and Piping*, **145**, 29-40 (2016)
- 9. S.S. Schulze, E.C. Fischer, S. Hamideh, H. Mahmoud, Wildfire impacts on schools and hospitals following the 2018 California Camp Fire, *Natural Hazards*, **104**(1), 901-925 (2020)
- 10. P.J. Camilleri, C. Healy, E.M. Macdonald, S. Nicholls, J. Sykes, G. Winkworth, M. Woodward, Recovery from bushfires: The experience of the 2003 Canberra bushfires three years after, (2010)
- 11. S.E. Quiel, T. Yokoyama, L.S. Bregman, K.A. Mueller, S.M. Marjanishvili, A streamlined framework for calculating the response of steel-supported bridges to open-air tanker truck fires, *Fire Safety Journal*, **73**, 63-75 (2015)
- 12. T. Kiran, N. Anand, M.E. Mathews, A.D. Andrushia, R. Walls, B. Kanagaraj, Post-fire behaviour and improving the performance of hot rolled open sections subjected to standard fire exposure, *Case Studies in Construction Materials*, **16**, e01021 (2022)
- 13. H.U. Sajid, R. Kiran, Post-fire mechanical behavior of ASTM A572 steels subjected to high stress triaxialities, *Engineering Structures*, **191**, 323-342 (2019)
- 14. H.U. Sajid, D.L. Naik, R. Kiran, Microstructure–Mechanical Property Relationships for Post-Fire Structural Steels, *Journal of Materials in Civil Engineering*, **32**(6), 04020133 (2020)
- 15. M. Bajpai, V. Shukla, F. Habib, Development of a heat resistant UV-curable epoxy coating, *Progress in organic coatings*, 53(4), 239-245 (2005)
- 16. P. Fauchais, A. Vardelle, Thermal sprayed coatings used against corrosion and corrosive wear, *Advanced plasma spray applications*, **10**, 34448 (2012)
- 17. C. Gaigl, M. Mensinger, Hot dip galvanized steel constructions under fire exposure, *IFireSS* 2017, 557-564 (2017)
- 18. M. William, G.P. J, S.A. M, Performance of Protective Coatings on Small Steel Bridges Subject to Bushfires, 8th Australian Small Bridge Conferenceed., 2017, p 1 to 25
- 19. R.D. Yasoda, Y. Huang, R. Kiran, X. Qi, Post-fire Performance of Wire-arc-Sprayed Zn-15Al Coatings, *Journal of Thermal Spray Technology*, 1-17 (2023)
- 20. R. Divya Yasoda, Y. Huang, Post-Fire Mechanical Properties of Thermally Sprayed Anti-Corrosive Coatings in Oil and Gas Pipelines, Pipelines 2022ed., p 203-210
- 21. W. Wang, T. Liu, J. Liu, Experimental study on post-fire mechanical properties of high strength Q460 steel, *Journal of Constructional Steel Research*, **114**, 100-109 (2015)
- 22. ASTM G99, Standard Test Method for Wear Testing with a Pin-on-Disk Apparatus, *Annual Book of ASTM Standards*, **3**, 401 (1999)
- 23. M. Li, Y. Li, F. Xue, X. Jing, A robust and versatile superhydrophobic coating: Wear-resistance study upon sandpaper abrasion, *Applied Surface Science*, **480**, 738-748 (2019)
- 24. L.A. Middlemiss, A.J. Rennie, R. Sayers, A.R. West, Characterisation of batteries by electrochemical impedance spectroscopy, *Energy Reports*, **6**, 232-241 (2020)
- 25. A. Ejbouh, A. Ech-chebab, S. Hassi, M. Galai, H. Benqlilou, M.E. Touhami, Durability assessment of LC3-based reinforced concrete under combined chloride-sulfate environment via the EIS technique, *Construction and Building Materials*, **366**, 130194 (2023)

- 26. M.S. Koochaki, R.E. Neisiany, S.N. Khorasani, A. Ashrafi, S.P. Trasatti, M. Magni, The influence of the healing agent characteristics on the healing performance of epoxy coatings: Assessment of the repair process by EIS technique, *Progress in Organic Coatings*, **159**, 106431 (2021)
- 27. C. Coogan, A. Rees, The nature of the thermal color change in zinc oxide, *The Journal of Chemical Physics*, **20**(10), 1650-1651 (1952)
- 28. P. Chung, M. Esfahani, J. Wang, P. Cook, Y. Durandet, Effects of heat treatment on microstructure evolution and corrosion performance of mechanically plated zinc coatings, *Surface and Coatings Technology*, 377, 124916 (2019)
- 29. K. Berent, J. Pstruś, T. Gancarz, Thermal and microstructure characterization of Zn-Al-Si alloys and chemical reaction with Cu substrate during spreading, *Journal of Materials Engineering and Performance*, **25**, 3375-3383 (2016)
- 30. M.M. Hasan, A. Sharif, M.A. Gafur, Characteristics of eutectic and near-eutectic Zn–Al alloys as high-temperature lead-free solders, *Journal of Materials Science: Materials in Electronics*, **31**(2), 1691-1702 (2020)
- 31. C. Rousseau, F. Baraud, L. Leleyter, O. Gil, Cathodic protection by zinc sacrificial anodes: Impact on marine sediment metallic contamination, *Journal of hazardous materials*, **167**(1-3), 953-958 (2009)
- 31. T. Polcar, A. Cavaleiro, High temperature properties of CrAlN, CrAlSiN and AlCrSiN coatings–Structure and oxidation, *Materials Chemistry and Physics*, **129**(1-2), 195-201 (2011)
- 32. R.H. Galib, A. Sharif, Development of Zn-Mg alloys as a degradable biomaterial, C Int Publ Adv Alloy Compd, (2016)
- 33. K. Sharma, S. Chatha, H. Sidhu, H. Singh, Heat Treatment of Thermal Spray Coatings: A Review, Proceedings of the National Conference on Advancements and Futuristic Trends in Mechanical and Materials Engineering, 2011
- 34. S. Liu, Y. Zhu, X. Lai, X. Zheng, R. Jia, X. Yuan, Influence of different heat treatment temperatures on the microstructure, corrosion, and mechanical properties behavior of Fe-based amorphous/nanocrystalline coatings, *Coatings*, **9**(12), 858 (2019)
- 35. S. Khandanjou, M. Ghoranneviss, S. Saviz, The investigation of the microstructure behavior of the spray distances and argon gas flow rates effects on the aluminum coating using self-generated atmospheric plasma spray system, *Journal of Theoretical and Applied Physics*, **11**, 225-234 (2017)
- 36. A.B. Bhalerao, R.N. Bulakhe, P.R. Deshmukh, J.-J. Shim, K.N. Nandurkar, B.G. Wagh, S.P. Vattikuti, C.D. Lokhande, Chemically synthesized 3D nanostructured polypyrrole electrode for high performance supercapacitor applications, *Journal of Materials Science: Materials in Electronics*, **29**, 15699-15707 (2018)
- 37. A. Amirudin, D. Thieny, Application of electrochemical impedance spectroscopy to study the degradation of polymer-coated metals, *Progress in organic coatings*, **26**(1), 1-28 (1995)
- 38. A. Bahgat Radwan, C.A. Mannah, M.H. Sliem, N.H.S. Al-Qahtani, P.C. Okonkwo, E. Berdimurodov, A.M. Mohamed, A.M. Abdullah, Electrospun highly corrosion-resistant polystyrene–nickel oxide superhydrophobic nanocomposite coating, *Journal of Applied Electrochemistry*, **51**(11), 1605-1618 (2021)
- 39. V. Barranco, S. Feliu Jr, S. Feliu, EIS study of the corrosion behaviour of zinc-based coatings on steel in quiescent 3% NaCl solution. Part 1: directly exposed coatings, *Corrosion Science*, **46**(9), 2203-2220 (2004)
- 40. S. Djerourou, H. Lahmar, N. Bouhellal, Y. Mebdoua, Study of twin wire arc sprayed zinc/aluminum coating on low carbon steel substrate: application to corrosion protection, Advanced materials research, 2013, Trans Tech Publ, pp 271-276
- 41. A. Farooq, M. Hamza, Q. Ahmed, K.M. Deen, Evaluating the performance of zinc and aluminum sacrificial anodes in artificial seawater, *Electrochimica Acta*, **314**, 135-141 (2019)
- 42. H.-S. Lee, J.K. Singh, M.A. Ismail, C. Bhattacharya, A.H. Seikh, N. Alharthi, R.R. Hussain, Corrosion mechanism and kinetics of Al-Zn coating deposited by arc thermal spraying process in saline solution at prolong exposure periods, *Scientific reports*, **9**(1), 1-17 (2019)
- 43. T.Q. Nguyen, C. Breitkopf, Determination of diffusion coefficients using impedance spectroscopy data, *Journal of The Electrochemical Society*, **165**(14), E826-E831 (2018)
- 44. M.B. Kannan, C. Moore, S. Saptarshi, S. Somasundaram, M. Rahuma, A.L. Lopata, Biocompatibility and biodegradation studies of a commercial zinc alloy for temporary mini-implant applications, *Scientific reports*, 7(1), 15605 (2017)
- 45. O. Schneider, R. Kelly, Localized coating failure of epoxy-coated aluminium alloy 2024-T3 in 0.5 M NaCl solutions: Correlation between coating degradation, blister formation and local chemistry within blisters, *Corrosion science*, **49**(2), 594-619 (2007)
- 46. Z. Wang, J. Zhang, X. Liu, J. Liu, G. Liu, Failure mechanism of plasma sprayed Tb-YSZ coating under NaCl high-low temperature cyclic corrosion, *Surface and Coatings Technology*, 129244 (2023)
- 47. G. Binal, Isothermal oxidation and hot corrosion behavior of HVOF sprayed 80Ni-20Cr coatings at 750° C, Surface and Coatings Technology, **454**, 129141 (2023)
- 48. J.G. Odhiambo, W. Li, Y. Zhao, C. Li, Porosity and its significance in plasma-sprayed coatings, *Coatings*, **9**(7), 460 (2019)

**Disclaimer/Publisher's Note:** The statements, opinions and data contained in all publications are solely those of the individual author(s) and contributor(s) and not of MDPI and/or the editor(s). MDPI and/or the editor(s) disclaim responsibility for any injury to people or property resulting from any ideas, methods, instructions or products referred to in the content.